Review Article

Yuhang Ren, Hongguang Wang*, Zhongzhi Guan, and Kainan Yang

Evaluation of the properties and applications of FRP bars and anchors: A review

https://doi.org/10.1515/rams-2022-0287
received August 31, 2022; accepted November 08, 2022

Abstract: The performance deterioration of steel anchors caused by steel corrosion is becoming more serious in slope anchorage applications. Therefore, the fiber reinforced plastic (FRP) composites have become a substitute material for traditional anchorage structures due to their advantages of low price, lightweight, high strength, and corrosion resistance. Numerous studies have proven that FRP anchors have better anchoring capacity than traditional steel anchors in practical engineering and are not as susceptible to environmental influences. This review mainly introduced the mechanical properties of FRP, focuses on the current research progress and innovation of FRP anchor in anchorage engineering, then provides a basis for the design of FRP anchor. In this study, the failure characteristics and problem of insufficient bonding strength of the first interface of FRP anchor anchoring slope were discussed, and the improvement was introduced. It will be conducive to the extension and application of FRP composites as structural materials in civil engineering. A detailed introduction is also given to biomaterials, which are mainly derived from nature and which will not only reduce waste disposal problems and environmental pollution but will also replace conventional applications. Finally, there will be an important reference and value for the development of green and sustainable engineering structures.

Keywords: polymer–matrix composites, mechanical properties, environmental degradation, microstructural analysis, biological polymer

*** Corresponding author: Hongguang Wang,** School of Civil Engineering, Northeast Forestry University, Harbin 150040, China, e-mail: wanghongguang@nefu.edu.cn
Yuhang Ren: School of Civil Engineering, Northeast Forestry University, Harbin 150040, China, e-mail: renyuhang@nefu.edu.cn
Zhongzhi Guan: School of Civil Engineering, Northeast Forestry University, Harbin 150040, China, e-mail: 2399925218@nefu.edu.cn
Kainan Yang: School of Civil Engineering, Northeast Forestry University, Harbin 150040, China, e-mail: ykn2020@nefu.edu.cn

1 Introduction

Composites are the combination of two or more materials, in which one of the materials is the reinforcing phase (polymer, metal, or ceramic). Composite materials are usually classified by the type of reinforcement such as polymer composite, cement, and metal matrix composite. Polymer matrix composites are mostly commercially produced composites in which resin is used as the matrix. The polymer matrix is classified into two types, thermoplastic and thermoset [1,2]. The main advantage of composite materials is their high tensile strength. Fire-, mildew-, and moth-proof properties along with high-temperature resistance, electrical insulation performance, and chemical stability are also very excellent. Composites also have disadvantages, mainly because they are two-phase materials. The combination of two different materials always induces internal stress, which causes an electrochemical reaction. This makes the composite more exposed to the environment than any single material. The difference in thermal expansion coefficient will cause warping, plastic deformation, and cracking. The fiber reinforced plastic/polymer (FRP) production methods are mainly categorized into autoclave and out-of-autoclave methods. The former involves the use of autoclaves that can produce high-quality FRP composites but with higher operating and energy costs, while the latter is more economical and does not require such a high level of equipment. FRP composites possess interesting properties like high specific strength and stiffness, good fatigue performance and damage tolerances, low thermal expansion, non-magnetic properties, corrosion resistance, and low energy consumption during fabrication [3,4]. The fiber content of FRP bars is generally 70–80%, and the resin accounts for 20–30%. With the larger fiber content, the stronger the FRP is, the more difficult it is to extrude [5].

FRP bars generally include basalt fiber reinforced polymer (BFRP) bars, carbon fiber reinforced polymer (CFRP) bars, glass fiber reinforced polymer (GFRP) bars, and aramid fiber reinforced polymer bars [6]. BFRP bar is a new type of nonmetallic composite material made of basalt fiber as reinforcement material and synthetic resin

as matrix material by pultrusion process and special surface treatment. Basalt fiber is an environmentally friendly fiber, its production process is from basalt fiber extraction and winding, composed of pyroxene and olivine. According to the alkalinity of basalt rock, the BFRP composites are categorized as alkaline basalts (up to 42%), mildly acidic basalts (43–46%), and acidic basalts (more than 46%) [7]. Although the production process of basalt fiber is very similar to that of glass fiber, basalt fiber does not require any additives and requires less energy [8,9]. FRP is a new material suitable for civil engineering in an environment of low carbon and environmental protection. The tensile strength of basalt fiber is around 2,000–4,500 MPa, higher than that of glass fibers, and the corrosion resistance of basalt fiber is excellent. In addition to resistance to acids, alkalis, and salt solutions, basalt fibers have the advantage of being UV resistant, a property not found in other FRP fibers. Basalt fiber is therefore one of the most promising new materials available to replace glass fiber [10].

GFRP bar is a composite material made of high-strength glass fiber as reinforcement material, synthetic resin as matrix material, and mixed with an appropriate auxiliary agent, through pultrusion and winding. Glass fiber is the most economical of the FRP fibers and it has a very good elongation, with E-glass elongation around 4.8% and S-glass elongation around 5.2–7%. However, apart from the advantage of high elongation, the other properties of glass fibers are inferior to those of other FRP fibers, for example, the tensile properties are lower than those of basalt and carbon fibers, and the corrosion resistance is far inferior to those of the above two fibers. The low modulus of elasticity also tends to limit the use of its high elongation as an advantage. CFRP tendons are usually composed of carbon fiber and matrix resin through a pultrusion process, creating a type of single arrangement fiber-reinforced composite. The matrix resins for fiber impregnation are normally thermosetting, such as polyester, vinyl ester, epoxy, phenolic, or polyurethane [11,12]. Although CFRP is an anisotropic material, CFRP tendons can be considered orthotropic materials. Carbon fiber is currently recognized as the best performing FRP fiber in the world, with a tensile strength of 3,530–6,600 MPa and a modulus of elasticity of 230–324 GPa. Although the modulus of elasticity of carbon fiber is very high, it has some defects due to its very low elongation of 1.5–2.0%, which is mainly due to the inherent small breaking strain of carbon fiber. And in addition to these drawbacks, the cost of carbon fiber is very high, so it is generally recommended for major projects. At present, due to the different fiber contents, the mechanical properties of FRP cannot be uniform, so it is suggested that the content standard of FRP should be gradually established and unified in the future.

Finally, a sustainable and clean manufacturing material is proposed, which is bio-based material. It is mainly derived from nature and waste materials, which is crucial to the sustainable development of the development industry. Using natural fibers will not only reduce waste disposal problems, but also reduce environmental pollution. Its low cost and recyclability are also significant. In the automotive industry, for example, natural fiber materials are used for their excellent thermal and acoustic insulation properties. The good thermal stability of palm and olive fibers among the natural fibers used in the mechanical and electrical industry also theoretically proves their suitability for a wide range of mechanical and electrical applications.

2 Mechanical properties of FRP bars in different environments

2.1 Bonding characteristics of fiber to matrix

The fibers have good compatibility with the polymer matrix material. The former is generally used as the load-carrying medium and the latter is to distribute the load uniformly throughout the reinforcement. The matrix system also protects the fibers from abrasion and impact damage as well as severe environmental conditions, such as water, salts, and alkalis [13,14]. The breaking load of FRP bar specimens made with phenolic matrix resin have higher heat resistance [15]. However, the matrix and fiber will also have premature debonding. Premature separation of FRP composites from the substrate usually occurs at about 30–60% of the rupture strain of FRP composites. In terms of shear strength of FRP bars, the effect of resin is not obvious. Wang *et al.* [16] concluded in the shear failure test of FRP bars that in the shear strength of FRP bars, the resin only accounts for 8% of the total strength, and only works in the first stage (the first stage is the simultaneous use of fiber and resin at the same time). The resin matrix also has a certain water absorption capability, which also leads to the diffusion of water in the material. In general, Fick's law does not apply to describe the diffusion of water in polymer materials, because when matrix cracks appear inside the polymer material, non-Fick's law diffusion is common. The Langmuir model considers both water-bound and unbound stages, and

moisture absorption along the fiber–matrix interface reduces the bonding strength of the interface, resulting in a loss of microstructural integrity. And hydrothermal aging may cause chemical and structural changes in the resin matrix, thereby affecting the properties of fiber-reinforced composites. Therefore, temperature and humidity are two important factors affecting the matrix. The plasticization of the matrix reduces the modulus of the matrix, and the mechanical degradation is the result of the expansion strain of the matrix. However, the sensitivity of the composite material to the strain rate is mainly caused by the matrix, and further studies on environmental changes and loading speed are needed.

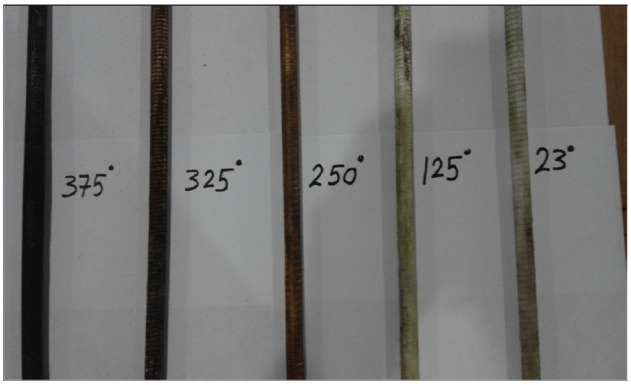

Figure 1: FRP bars before and after exposure to different high temperatures [22].

2.2 Applicable temperature range of FRP bar composites

FRP has high-temperature exposure and can be used at very low temperatures around −200°C to relatively high temperatures around 600–800°C [17,18]. The weight gain of FRP at 80°C is approximately three times greater than that at 20°C [19]. In general, the mass loss of FRP occurs at 200–450°C. The variation in FRP mass with temperature was measured by TGA. The sharp decline in FRP mass is mainly between 300 and 450°C. That is an 18% drop, which is because of the thermal degradation of the polymer [20]. In the study of the high-temperature resistance of the three kinds of fibers, BFRP, CFRP, and GFRP, their strength is influenced on being kept at 200°C for 2 h. After being kept at 600°C for 2 h, only BFRP retains volume integrity and 90% strength [21].

There are two stages in the thermal decomposition process of FRP bars, and the reaction modes are different. In the first stage, the matrix is rapidly decomposed [21] into the corresponding residue and a part of gas, and in the second stage, the residue is slowly decomposed. The thermal stability of BFRP is better than that of GFRP, which is mainly due to the presence of FeO and Fe_2O_3 in BFRP, which makes BFRP to have very superior dissolution characteristics, reduces heat conduction, and improves temperature stability. For example, as shown in Figure 1, the testing temperature increases from right FRP to left ones. It is observed through visual inspection that the color of specimens changed from slight yellowish-green to nigger-brown at elevated temperatures, which was induced by the oxidation and decomposition of a matrix [22]. And Figure 2 also shows that thermal degradation occurred at these temperatures, and the molecular chains of the polymer broke, resulting in the formation of microcracks both at the fiber/matrix interface and in the matrix phase.

FRP composites may encounter high temperature or even fire during their service life. The mechanical properties of FRP are usually very sensitive to temperature, and the degradation reason is generally attributed to the degradation of the resin matrix. At present, most literatures focus on the effect of temperature on the mechanical properties of FRP bars, but there is little literature on preventing the loss of mechanical properties of FRP bars at high temperature. For example, when the ambient temperature exceeds the resin glass transformation temperature (T_g), the resin is softened and cannot efficiently transfer the stress between the fibers. It results the decreasing in the synergistic effect between the fibers and the resin matrix. When the ambient temperature exceeds the thermal decomposition temperature of the resin (T_d), the resin will decompose, the fiber between the lack of constraints, and the mechanical properties of FRP will sharply decline or even fail. In the tensile, shear and bending curves of FRP bars, the mechanical properties of FRP bars do not change from −40 to 50°C [20]. At temperatures below −50°C, the molecular chains' mobility of the polymer decreases, increasing the mechanical stresses required for rupturing the material. Below T_g (around 120°C), the matrix is in a glassy state. When increasing the temperature and reaching the decomposition region, the breaking of molecular bonds starts and the ductility of the material increases, leading to a decrease in mechanical strength and stiffness of the material [23–26]. At temperatures over 300°C, the polymer has undergone strong degradation (combustion, oxidation) and load transfer provided by the matrix is severely reduced [26,27]. It is suggested that the research should be carried out from the aspect of the matrix. For example, the reason for the poor high temperature resistance of epoxy

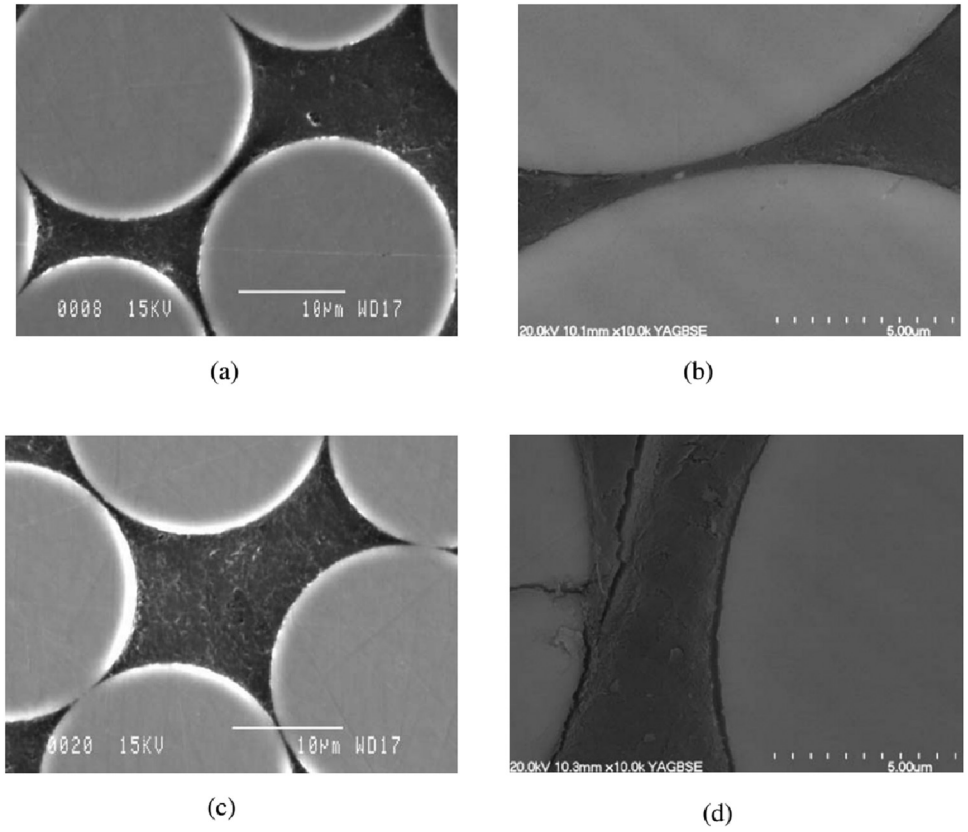

Figure 2: Micrographs of transversal fiber/matrix interface: a) the polymer matrix, the glass fibers and the interface between the fibers and matrix for an unconditioned reference specimen, b) a dry specimen conditioned at −100°C, c) a specimen saturated in water without any subsequent conditioning, and d) a specimen saturated with water and conditioned at −100°C for two hours [20].

resin commonly used in FRP bars is that it contains polar groups such as hydroxyl groups. The methods to improve it are mainly modification and copolymerization, among which common polymers for epoxy resin modification include polyurethane, polyimide, bismaleimide, and polysulfone. Copolymerization mainly utilizes the reactive groups in the molecule of the modified material to react with the epoxy groups and hydroxyl groups in the epoxy resin to form a tree or copolymer. Thereby a stable heat-resistant structure is introduced into the curing system.

The size of elongation generally reflects the ultimate deformation capacity of materials. Some scholars have obtained the influence curve of temperature on the elongation of FRP bars through a series of tests. Temperature has a great influence on the elongation of FRP bars. At 183 days, the elongation retention of FRP bars is 67.84% at 40°C, 51.05% at 60°C, and 34.97% at 80°C. This phenomenon is more and more obvious as time goes on [28,29]. These scholars only demonstrated the effect of temperature on elongation through tests, but did not propose specific improvements, such as blending fibers to form composite fiber reinforcement, the mechanism of which is to blend high ductility fiber with low ductility fibers to improve the overall ductility of the material.

2.3 Tensile modulus of FRP bars

Elastic modulus is an important physical quantity in FRP composites. By analyzing the elastic modulus of FRP, the durability of corresponding fiber composites can be obtained, and the degradation model of mechanical properties of fiber composites can be established on this basis. The diameter of FRP is the main factor affecting the elastic modulus of FRP. The experimental conclusions obtained by Gu *et al.* [30] are completely contrary to those obtained by Huo and Zhang [31], the former considers that the elastic modulus of FRP bars decreases with the increase in the diameter of FRP bars, while the latter considers that the elastic modulus of FRP bars increases with the increase in the diameter of FRP bars. The

former believes that the main reason for this phenomenon is that the mechanical properties of bars generally depend on the weakest link of random distribution, but with the direct increase in the number of specimens, the distribution defects will also increase, which will lead to the decrease in the elastic modulus of FRP bars. The latter demonstrates its conclusion as shown in Figure 3, the elastic modulus of FRP bars increases with the increase in the diameter of FRP bars. The reason for this difference may be related to the inconsistent content of fiber and matrix in FRP tendons. The tensile modulus of elasticity of FRP is calculated as follows.

$$E_b = K_1[E_f V_f + E_m(1 - V_f)], \quad (1)$$

where E_b is the tensile modulus of FRP bars; E_f and E_m are the tensile elastic modulus of FRP and matrix, respectively; V_f is the FRP volume fraction; K_1 is mainly related to the interfacial strength, the bonding strength between the fiber and matrix, the arrangement, distribution, and fracture mode of the fiber.

The elastic modulus of BFRP bars is 35–42% higher than that of GFRP bars but is 1/4 of the elastic modulus of steel bars [32]. Although the elastic modulus of FRP bars is low, its elastic modulus is quite stable, almost not affected by wet, acid, alkali, and salt environment [33]. The elastic modulus of FRP bars can be significantly improved by mixing some steel wires into the FRP bars. The new bars after mixing are called FRP wire composite bars (BFSWC). It can be seen that the content of steel wire increases from 4 to 24%, and the elastic modulus of FRP bars increases by 18.4, 36.3, 66.96, and 86.05%, respectively. And after adding a certain steel wire, the new BFSWC reinforcement will also have partial ductility [30,34].

The increase in temperature also affects the stability of elastic modulus. It can be seen from Figure 4 that the elastic modulus of FRP bars at 200°C decreases by 4.7, 1.8, and 16.3% at 0,1, and 2 h, respectively. It can be concluded that the higher the temperature, the more obvious the effect of holding time on the elastic modulus of FRP bars [35]. However, it does not consider the critical temperature in the study. When the temperature is small, the elastic modulus of FRP has little effect, and when the temperature is high, the elastic modulus of FRP decreases sharply. This shows that there may be a critical temperature to affect the elastic modulus of FRP. In the future research, we should focus on the change law of elastic modulus when the temperature is large, and find a relatively accurate temperature critical value.

2.4 Tensile strength of FRP bars

The longitudinal tensile strength of BFRP is very high. Its tensile strength is higher than that of ordinary steel bars and GFRP bars, and the tensile strength is about twice that of ordinary steel bars [36,37]. The tensile strength of CFRP bars is greater than that of BFRP bars. The longitudinal (parallel to the fiber direction) properties of FRP bars are mainly of fiber, while the transverse (perpendicular to the fiber direction) properties are mainly of resin. As the stress–strain curve of FRP bars is a straight line,

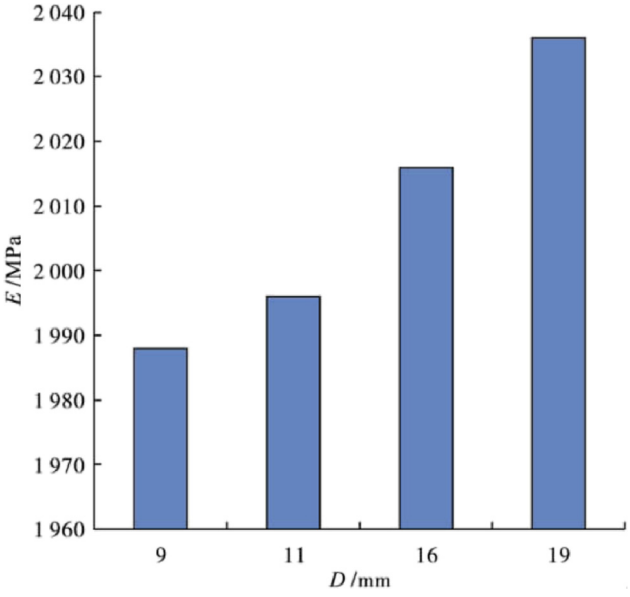

Figure 3: Tensile elastic modulus of the FRP bars with different diameters [31].

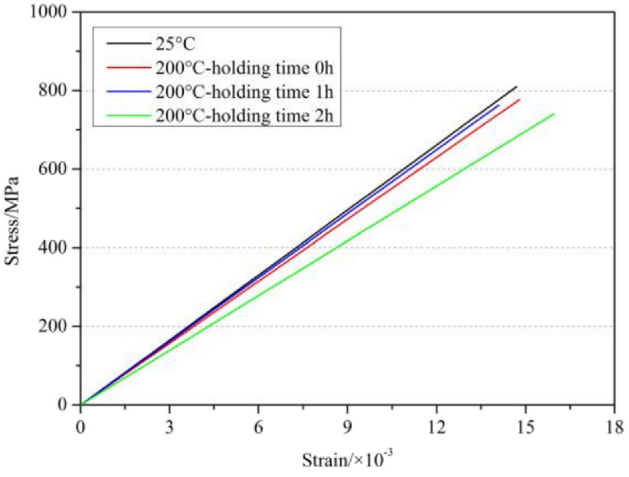

Figure 4: Stress–strain curve of FRP bars after elevated temperature exposure: at 200°C [35].

there is no yield step, brittle failure will occur when a failure occurs, so sufficient strength and safety reserve of FRP bars should be provided [38–40]. Therefore, given a term as the standard value of tensile strength, the standard value of tensile strength of FRP bars is 80% of the ultimate tensile strength, the standard value of tensile strength is also known as the nominal yield strength, and its formula is as follows [41]:

$$f_{\mathrm{fu},k} = -1.65\sigma, \tag{2}$$

$$f_k = 0.8 f_{\mathrm{fu},k}, \tag{3}$$

where $f_{\mathrm{fu},k}$ is the ideal strength of FRP bars; $f_{\mathrm{fu,a}}$ is the average value of measured ultimate tensile strength of FRP bars; σ is the standard variance of the average test value of FRP bars; and f_k is the standard value of tensile strength.

At present, FRP is regarded as a new type of high-strength anchorage material in the field of anchorage, mainly because of its high-strength tensile property, but under high temperature, the tensile property of FRP composites will be seriously affected. When held at 100°C for 1 h, the tensile strength degradation rate of FRP bars is 0.5%, and the tensile strength degradation rate of FRP bars is 1.2% for 2 h. When held at 200°C, the tensile strength degradation rate of FRP bars is 5.8% for 1 h, and the tensile strength degradation rate of FRP bars is 8.5% for 2 h. At 300°C, the tensile strength degradation rate of the FRP bars held for 1 h is 21.2%, and that of the FRP bars held for 2 h is 28%, It can be seen from the data that when the temperature is low, the effect of holding time on the tensile strength degradation rate of FRP bars is not obvious, but with the increase in temperature, the effect of holding time on the tensile strength degradation rate of FRP bars will become very obvious [35,42].

However, most of the tests, like the above, only study the degradation law of mechanical properties under the action of a single tensile force at high temperature, and do not consider the change law of mechanical properties under the simultaneous action of tensile and shear force, which is inconsistent with actual engineering. The characteristics of the actual engineering situation should be restored. For example, FRP is often used in the use of anchors in slope support because of its high tensile properties. The stress characteristics of the anchors are not only tensile force, but tensile force and shear force appear at the same time. It should make more research on the degradation of mechanical properties under simultaneous tensile-shear action at high temperatures and prevention by increasing the fibers. This is because under the action of high temperature, the damage of FRP bars is from the surface to the inside. The smaller the diameter of the FRP, the larger the relative damaged section. At the same time, the monotonic load test shows that the driving shear performance parameter of FRP bars is the fiber content. Their shear capacity increases approximately linearly with the fiber content.

And in the tensile test of FRP reinforcement, it can be observed that with the increase in stress, the first matrix loss occurs on the surface of FRP reinforcement. This is because some of the bond strength between the fiber and matrix drop due to the rupture, and fiber breakage can be heard, with further increase in stress, the decline in bond strength between the fiber and matrix continues to accelerate, and white-spotted cracks appear on the surface of FRP bars until the FRP bars are destroyed. The failure mode of FRP bars is usually “lantern” type. The method for enhancing the adhesion between the fiber and the matrix is not mentioned in the article, and some supplements should be made to enhance the adhesion between the fiber and the matrix by a modified method. For example, when 1.5% mullite powder is added, the interface between the fiber and the matrix will be in a dense state. In addition, insufficient expansion of defects in FRP bars does not significantly affect the tensile properties of FRP bars [43].

2.5 Shear performance of FRP bars

Nowadays, the shear performance of FRP as anchor rod is considered to a greater extent in anchorage engineering. Due to the low shear strength of FRP, when it is used in anchorage structure, shear failure may occur when the FRP anchor rod does not fully exert its high tensile strength. The shear strength of FRP bars is inferior to that of steel bars. The shear strength of CFRP bars is about 1/12 to 1/8 of its tensile strength [44]. The main reason for the low shear strength of FRP bars is the single arrangement of fibers. The main method to improve the shear strength of FRP composites is to increase the diagonal arrangement of fibers [45]. Grafting graphene oxide and carbon nanotube on the surface of carbon fiber improved the interlaminar shear strength of the resulting composites by 83.39% [46,47]. In addition, increasing the diameter of FRP bars can also improve the shear strength of FRP bars [48]. The shear stress to shear deformation ratio indicates the characteristics of three stages. In the first stage, the fiber and resin work simultaneously resist the shear forces, and in the second stage, the resin fails

due to shearing and gradually stops providing shear resistance. In the final stage, the fibers resist shear force by themselves owing to their curvature at the shear planes [49].

At present, how to effectively improve the shear strength of FRP is still a promising research direction. In general, the main shear performance of FRP bars is contributed by the internal fibers, not affected by diameter and resin type. Therefore, in view of this characteristic, the most frequently proposed suggestion by global scholars is to mix FRP fibers. It can be seen from Figure 5 that the shear resistance of FRP bars is significantly improved after mixing. However, the smaller the fiber diameter, the more fiber content per unit volume, and the lower the fiber/resin interface bond strength [16].

Later scholars have concluded that when the shear force is less than or equal to 50% of the pure shear force, the axial tensile properties of FRP bars do not change significantly due to the sheer force. This can be interpreted as an elastic matrix, which allows lateral deformation and more direct force transfer through the fibers [50].

2.6 Compressive performance of FRP bars

2.6.1 Effect of slenderness ratio on compressive performance of FRP bars

FRP bars belong to anisotropic materials, its compressive strength is far less than its tensile strength, and the compressive performance test of FRP bars is not perfect, there is no set of mature specifications like its tensile test. Maranan *et al.* [51] found that the compressive strength of FRP bars is only 51.7% of the tensile strength when the elastic modulus is equal, and the slenderness ratio is an important factor affecting FRP bars. Deitz *et al.* [52] studied the influence of slenderness ratio of FRP bars on compressive performance by using the improved ASTM D695-10 test procedure. The results showed that when the cross section diameter was 15 mm, the compressive strength of the bars with low slenderness ratio was only 50% of the tensile strength, and the compressive strength was further increased with the increase in slenderness ratio.

2.6.2 FRP bars in compression damage mode

Three modes of failure such as crushing, buckling, and a combination of crushing and buckling (splitting) were observed in the FRP bars tested for compression, which were highly influenced by the Lu/db ratio (slenderness ratio).

The crushing failure mode is not related to the diameter of the FRP bars; all bars with lower Lu/db (2 and 4) have crushing failure, as shown in Figure 6.

The main damage pattern of combination of crushing and buckling is splitting between the fibers and significant damage in the matrix, which generally often occurs for Lu/db = 8 as shown in Figure 7, and this damage pattern is generally related to the modulus of elasticity of the FRP tendons. And the FRP bars with Lu/db = 8 shows an increased separation in the matrix with fiber fracture. In fact, this fits extremely well with the failure pattern of longitudinal reinforcement in actual concrete columns.

Khan *et al.* [53] also carried out compression tests on GFRP bars and CFRP bars having the same diameter to compare the compressive strength of the two types of

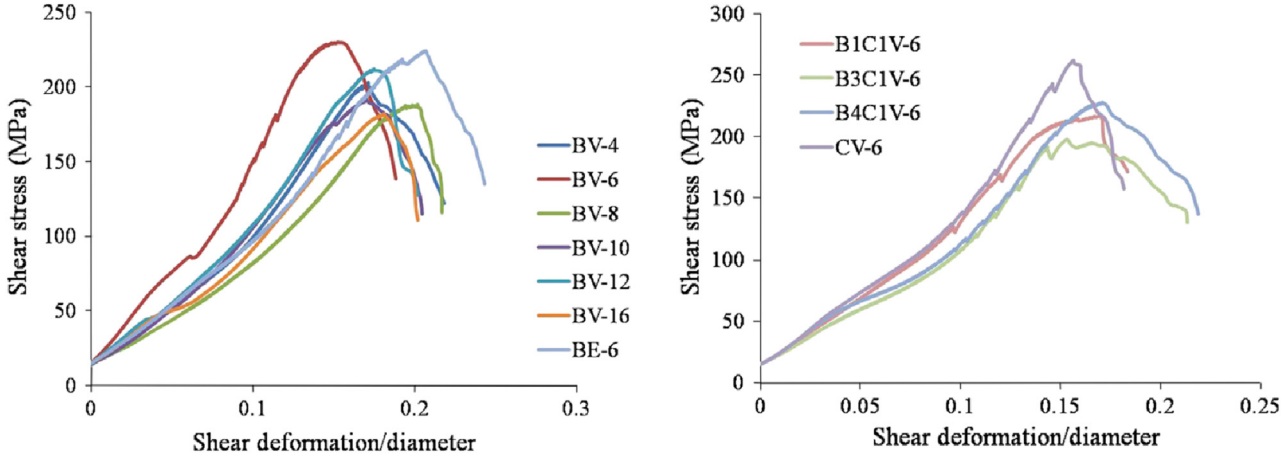

Figure 5: Stress–deformation curves: (a) BFRP rods and (b) CFRP and hybrid B/CFRP rods [16].

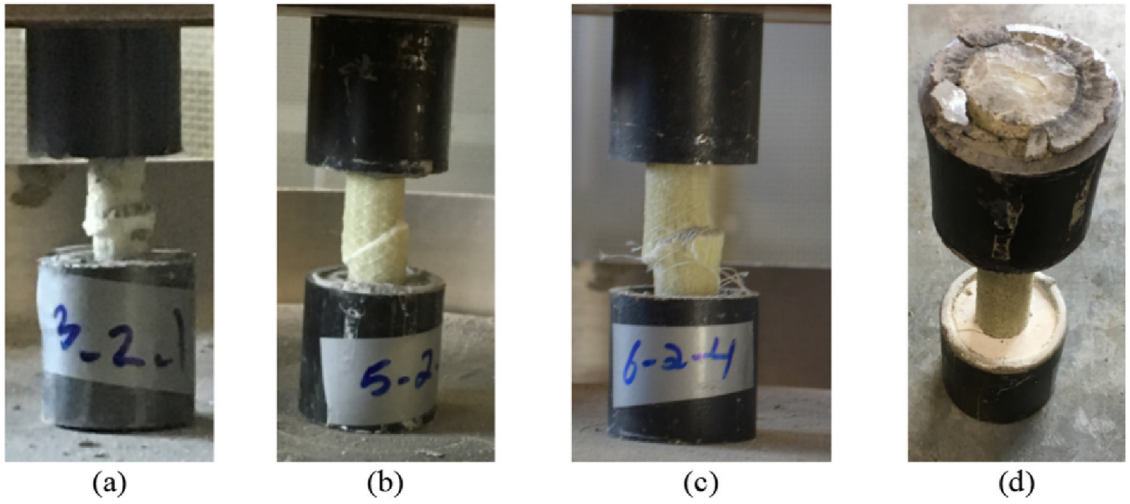

Figure 6: Mode of failure for bars with 2 and 4 Lu/db ratios for GFRP bar: (a) #3, (b) #5, (c) #6, and (d) premature failure [54].

fiber bars. As can be seen in Figure 8, both types of FRP bars failed due to fibers' separation, which may have been caused by the resin in the bars failing under pressure, rather than by the fibers yielding. As can be seen from Figure 9, the compressive performance of the GFRP bars is better than that of the CFRP bars, with an ultimate compressive strength of 1.4 times that of the CFRP bars and an ultimate compressive strain of 1.65 times that of the CFRP bars. However, this article only compares the compressive properties of the two types of bars and does not further investigate the mechanism. It is recommended that the microscopic morphology of the cross section of the two types of bars after compression damage should be observed by scanning electron microscope (SEM) to provide a theoretical basis for improving the compressive properties of FRP bars in the future. Buckling failure is also not related to the diameter of the tendon, and occurs regardless of the diameter of the bar when Lu/db = 16, as shown in Figure 10 [54].

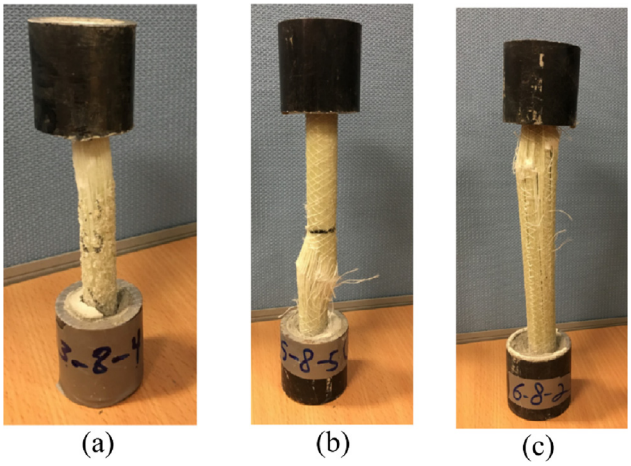

Figure 7: Mode of failure for GFRP bars with Lu/db of #8: (a) #3, (b) #5, and (c) #6 [54].

2.6.3 Test method and improvement of compressive strength of FRP bars

As there is no code or test standard available, the general consensus is to follow the ASTM D695 test procedure to determine the compressive properties of FRP bars. However, premature splitting of the FRP bars was observed during the

Figure 8: Observed failure modes in tested FRP bars: (a) GFRP and (b) CFRP [53].

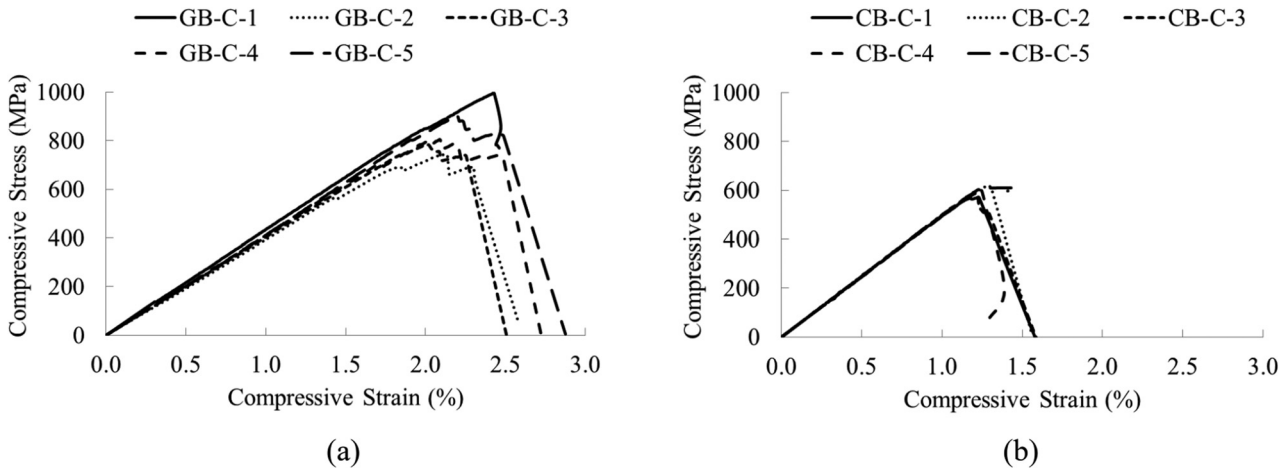

Figure 9: Compressive stress–strain of tested FRP bars: (a) GFRP bars and (b) CFRP bars [53].

tests, the mechanism of which was mainly due to the high stress concentration at the ends of the FRP bars during compression and the transfer of the stress to the entire FRP bar.

Method 1: Insert the end of the bar into the steel rod. The purpose of this test method is to take advantage of the fixed end conditions created by the rigid bars, but the disadvantage of this method is that there is a significant difference between the lateral stiffness of the FRP bars and the stiffness of the steel bars resulting in a vertical cut at the point of contact between the FRP bars and the bars [52,55], as shown in Figure 11.

Method 2: The ends of the tendons were epoxy sealed, but the softening behavior of the epoxy was not effective in confining the ends of the bars, resulting in many FRP bar specimens being damaged within the epoxy sealed area. On the other hand, the sealed ends of the top and bottom steel caps make the removal of the FRP bars difficult and their re-use is not suitable for the preparation or testing of the next sample. And this method is only used to test relatively short FRP bars, as shown in Figure 12.

Therefore, in order to accurately measure the compressive strength of FRP bars AlAjarmeh *et al.* [54]. investigated a new test method by adding covers at the top and bottom to allow the FRP bars to be placed vertically in the tester in the longitudinal direction and compressed by concentric applied loads, as shown in Figure 13.

2.7 The time-dependent effect of different FRP bars

While previous studies have focused extensively on the short-term time dependence of FRP rods, there are now a number of scholars who have conducted extensive

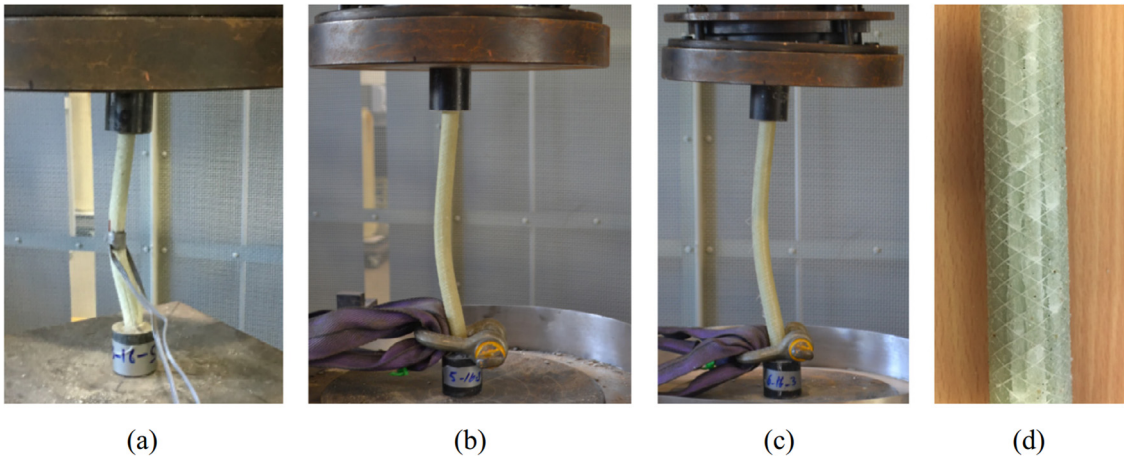

Figure 10: Mode of failure for GFRP bars with Lu/db of #16: (a) #3, (b) #5, (c) #6, and (d) surface crack [54].

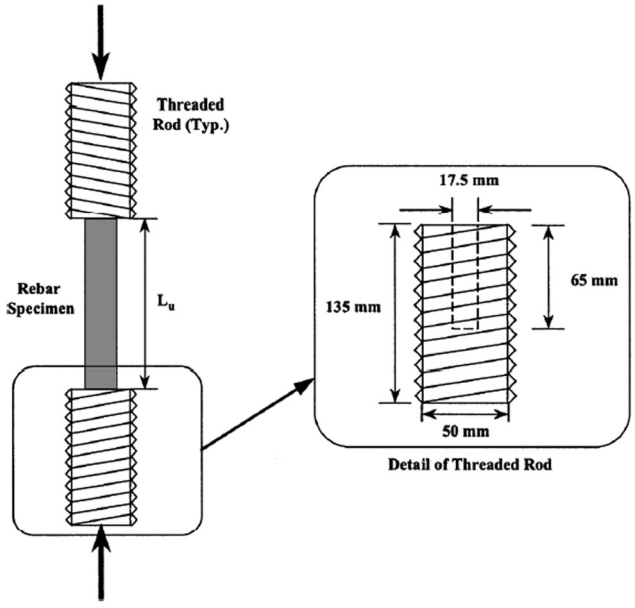

Figure 11: Available test method for compression test of GFRP bars [54].

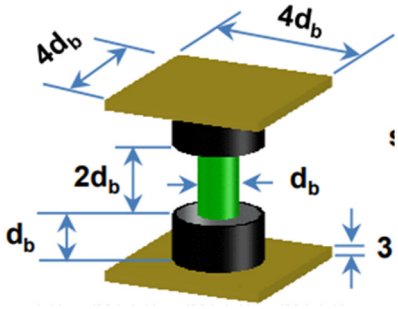

Figure 12: Test model of compression test of GFRP bars [54].

studies on the long-term time dependence of FRP rods, and they have studied in detail the time dependence of different types of FRP rods in different environments. They conclude that the parameters affecting the long-term time-dependence of FRP rods are the fiber and matrix properties. First of all, the matrix, generally used as FRP rod for polyester, vinyl ester and epoxy resin, which because of vinyl ester and polyester contain ester bond easy hydrolysis degradation, and epoxy resin does not contain ester bond, so the time dependent effect of epoxy resin when encountering water is better. Then, looking at the fiber part, when the GFRP fibers are exposed to an alkaline environment, the increase in exposure time largely reduces the residual strength of the GFRP fibers, whereas the increase in exposure time has a weak effect on the residual strength of the BFRP and CFRP fibers due to their good alkaline resistance, which

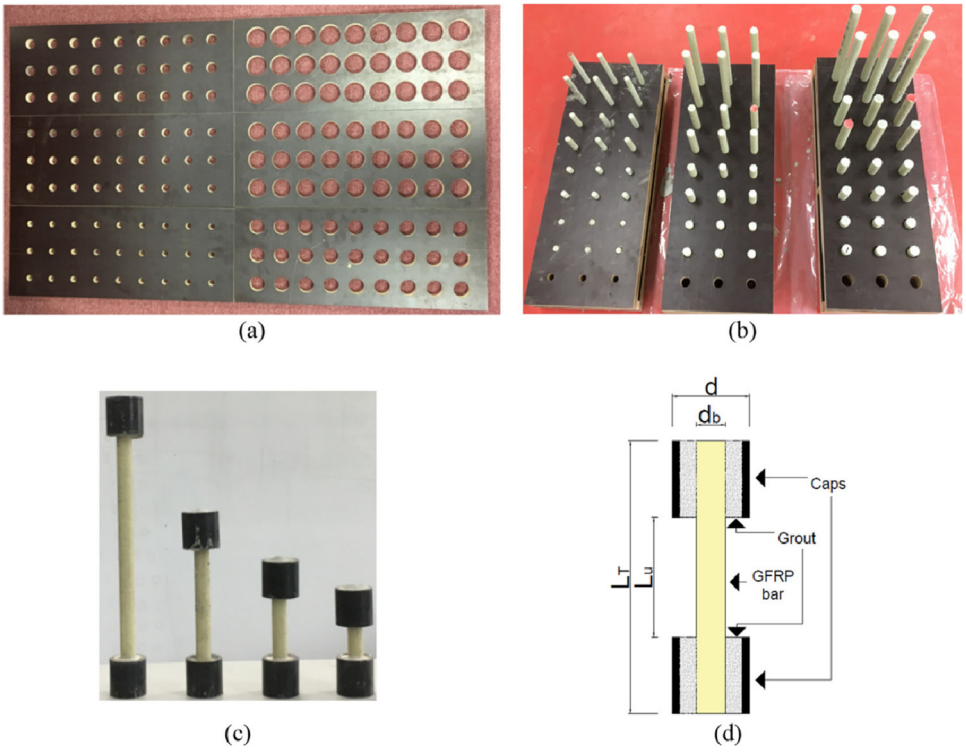

Figure 13: (a) Drilled plywood sheets for bars and caps, (b) fabricating bar samples in plywood molds, (c) samples prepared for testing, and (d) schematic diagram of the test specimen [54].

also shows the better durability of BFRP and CFRP compared to GFRP in an alkaline environment.

In wet conditions, the GFRP fibers also lose a lot of strength over time, up to 25% of their own strength. In contrast, the durability of GFRP increases significantly in cold environments and the strength even increases with time. The mechanism for this phenomenon is that GFRP fibers become stiffer in cold weather resulting in fewer pores. CFRP fibers do not lose more than 10% of their strength over time, except in alkaline environments, where there is almost no significant increase in strength loss over time. In the future, it will be even more necessary to study how the extension of time will affect the durability of FRP rods.

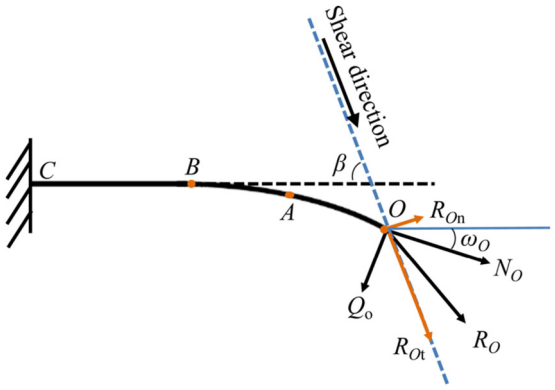

Figure 14: Force of anchor under shear action [57].

3 Performance and improvement method of FRP anchor in different environments

3.1 Analysis of shear strength variation and slip mechanism of FRP anchor

3.1.1 Variation characteristics of shear strength of FRP anchor

Assuming that the anchor presents linear elastic deformation along the axial direction, and the shear stress of the anchor/grouting interface is equal to the axial displacement of the anchor at the same position, it can be expressed as follows [56]:

$$\tau(s) = \frac{E_b D_b}{4} \frac{a}{b} e^{-\frac{s}{a}} \left(1 - e^{-\frac{s}{a}}\right), \tag{4}$$

where $\tau(s)$ is the shear stress of the anchor/grout interface; E_b is the Young's modulus of the rock anchor; D_b is the rock anchor diameter; a and b are the coefficients; and s the shear slippage of the anchor/grout interface.

In addition, as shown in Figure 14, the contribution of the anchor to the shear strength is a combination of the axial force and shear force, decomposing the axial force N_0 and the sheer force Q_0 parallel to the joint direction and perpendicular to the joint direction yields Rot and Ron, i.e., the components parallel and perpendicular to the joint, respectively. The former provides an increment of cohesive force to the rock joint, and the latter provides an additional normal load on the joint surface while increasing the friction on the joint surface. These behaviors are called the cohesive force enhancement effect and the friction enhancement effect, respectively. The shear strength contribution of the anchor is the sum of the two effects. Based on the Mohr–Coulomb criterion, the following formulas can be used to compute the shear force contribution of the rock anchor [57]:

$$\tau = C_b + \sigma_b \tan \phi_j, \tag{5}$$

$$C_b = N_0 \cos(\beta - \omega_0) + Q_0 \sin(\beta - \omega_0), \tag{6}$$

$$\sigma_b = N_0 \sin(\beta - \omega_0) - Q_0 \cos(\beta - \omega_0), \tag{7}$$

where τ is the shear strength contribution of the anchor; C_b is the additional cohesion of the anchor on the joint surface; σ_b is the additional normal force of the anchor on the joint surface; and ϕ_j is the joint friction angle.

The variation characteristics of shear strength of FRP bars can be divided into four stages, namely, the linear elastic stage, the nonlinear stage before peak value, the nonlinear softening stage, and the residual strength stage. For the FRP anchor anchored jointed rock mass test block, the curve before the peak increases linearly. After the peak value, the shear strength decreases slowly with the increase in shear deformation and presents a nonlinear attenuation trend in a long period of shear displacement. This is because when the specimen reaches the peak load, a large number of fiber composites at the joint plane dislocation can be fully extended, and the fiber absorbs a lot of energy in the process of shear or pulling, so it shows a certain toughness. The fibers siding in shear bearing capacity is caused by the accumulation of fiber siding and fiber material damage in the matrix.

With the increase in load, the peak value of the shear stress curve also increases. When the peak value of shear force is greater than the bonding strength of the first interface, the first interface shear failure will occur. As the load continues to increase, the shear stress peak also moves deeper. At the same time, shear stress affects the

shear failure depth of the bar and slurry more and more deeply [58].

The above literature discusses the influence of shear force on the failure of anchors in detail, but the method of enhancing the shear capacity of FRP anchors is lacking in the article. There are five methods to increase the shear strength of FRP anchors at home and abroad. The first method is to increase the diameter of the FRP anchor. Einstein *et al.* [59] analyzed the influence of the anchor diameter on the shear strength and found that the anchors with larger diameters have higher shear strength. The second method is to increase the amount of fiber appropriately. The driving shear performance parameter of FRP anchors is the fiber content. Their sheer capacity increases approximately linearly with the fiber content, provided the pullout failure is avoided by reasonably sizing the anchor, and the shear capacity of FRP anchors is independent of the embedment depth. The third method is to make the surface of the FRP anchor rough. It could be seen from Figure 15 that the shear strength of a rough joint surface FRP anchor is greater than that of a smooth joint surface FRP anchor under the same anchorage conditions.

And the fourth method is to increase the normal stress. Figure 16 shows that with other conditions unchanged, the shear strength increases with the increase in the normal stress, but the growth rate gradually slows down. This is because the larger normal stress increases the extrusion of the interface between the anchor and mortar, and thus restricts the promotion of shear strength of FRP anchor by axial force. As a result, the shear strength amplitude gradually slows down with the increase in normal stress.

The last method is to increase the angle between rock joints and FRP anchors. Under the same conditions, the shear strength of rock anchor increases with the increase in anchorage angle (the angle between rock joint and anchor). But Spang *et al.* [60] came to a different conclusion. The optimal anchorage angle of FRP anchorage specimens is less than 70°, which is because when the anchorage angle is large, the anchor is mainly subjected to more transverse shear stress. However, due to the weak shear strength of the FRP anchor, the peak shear strength of rock mass is relatively low. When the anchorage angle is small, the axial stress of the anchor can promote the shear strength of jointed rock mass, and part of the transverse shear effect is transformed into a tensile effect. At present, the research on the expansion anchor is not mature at home and abroad, and its main mechanism is to suppress the shear failure of the anchor by generating the phenomenon of negative Poisson's ratio. Most scholars focus on the research on FRP materials to enhance their shear strength, but the results obtained are not very optimistic. The domestic scholar Dai [61] has developed a fast-hardening micro-expansion high-strength bolt grouting material. Its shear resistance mechanism mainly uses alumite as an expansion agent. After a period of hydration reaction, ettringite can be formed, and it will be filled into the pores of the interface, while ettringite is so dense that the total porosity can vary from 3.14 to 0.7% with time. The expansion agents mentioned in this study contribute significantly to the anchoring of steel anchors, but the anchoring effect of expansion agents applied to hybrid FRP anchors has

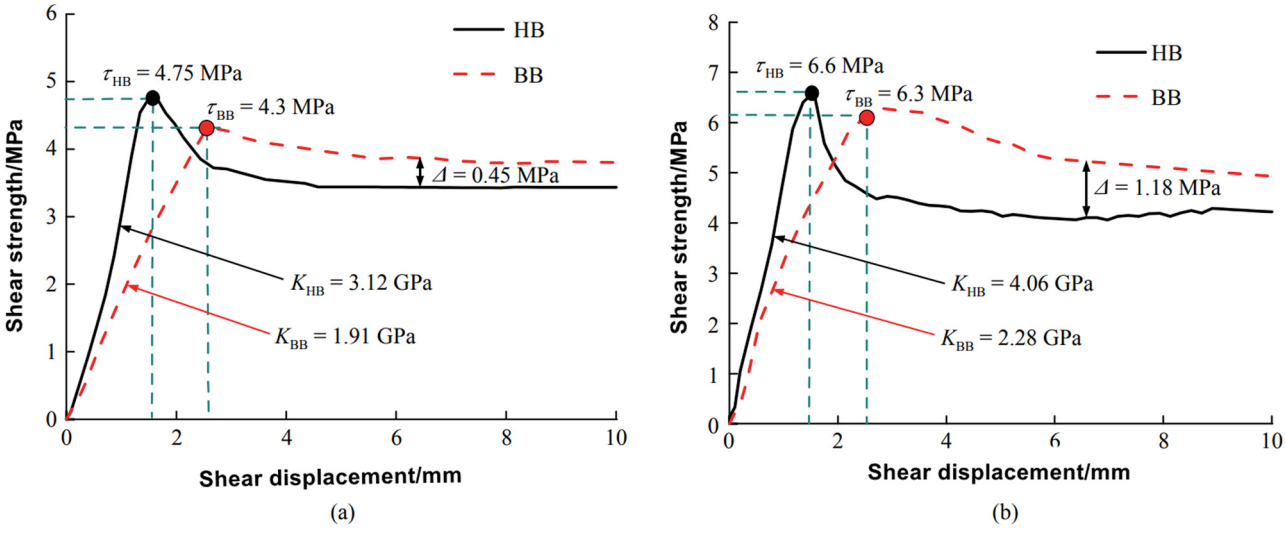

Figure 15: Shear strength displacement curve [36].

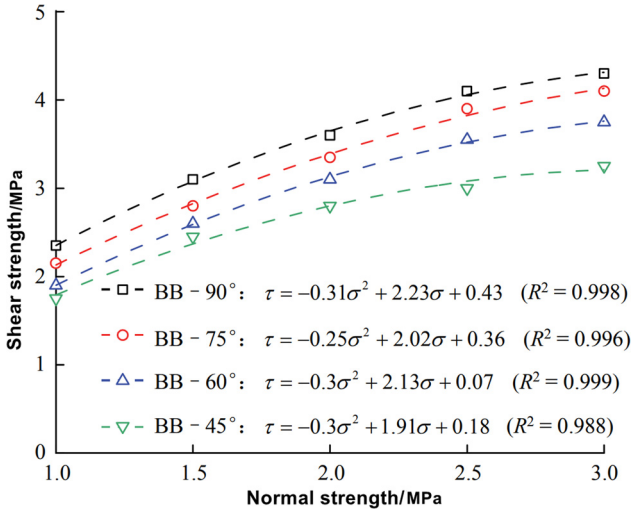

Figure 16: Relationship between shear strength and normal strength reinforced by BFRP anchor [36].

not been studied, so there are gaps in this area that need further research.

3.1.2 Slip mechanism analysis of FRP anchor

The main reason why FRP anchor is more prone to shear slip failure than steel anchor is the bonding force between FRP anchor and mortar. The small effective contact area between the anchor and the anchor mortar leads to the failure of the anchor interface before the drawing load increases to the tensile strength of the anchor, and the anchor is pulled out before failure [62]. It could be seen from Figure 17 that under different normal stresses, the energy is absorbed by FRP bars before the peak increases

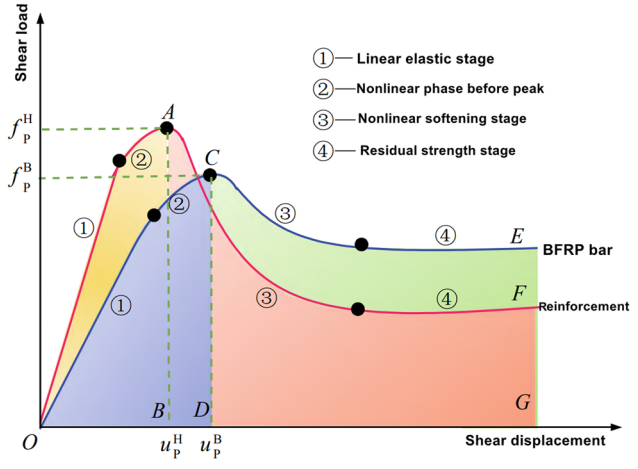

Figure 17: Schematic diagram of shear displacement characteristics of anchored jointed rock mass [36].

by 25, 38, 27, 20, 13, and 25% relative to that absorbed by steel bars before the peak. Although the shear strength of the FRP anchored rock mass is less than that of the steel bar anchored rock mass, as the FRP anchor-on joint rock anchorage shear displacement backward-shift, reaches the peak strength of the FRP anchor to absorb the energy, the more absorption of total energy and steel anchor absorption roughly within 10% of the total energy of amplitude. It can be seen that the FRP anchor can absorb more energy before the shear strength peak so that the ductility of the FRP anchor can be improved [36]. On the basis of its analysis of the FRP anchor, the grouting body can also be improved to a certain extent, and the interface bond strength of the FRP reinforcement can be improved from another idea to avoid slip damage. For example, a percentage of epoxy resin could be added to the mortar, and there is no literature on this idea. For one thing, epoxy has better bonding properties to FRP tendons, and for another, epoxy is an isotropic material that is inexpensive.

The free end displacement of anchor consists five parts: the elongations of anchor member, the amount of slip at the first interface and the second interface, the elastic deformation of mortar body and the elastic deformation of the rock mass. So, the expression for slip is as follows:

$$\delta_e = \delta_b + \delta_s + \delta_w + \delta_m + \delta_c, \tag{8}$$

where δ_e is the measured value of rod end displacement; δ_b is the elongation of the anchor member; δ_s is the amount of slip at the first interface; δ_w is the amount of slip at the second interface; δ_m is the elastic deformation of mortar body; and δ_c is the elastic deformation of rock mass.

Typical slip curves at the loading end can be divided into three stages: The first section is the sliding displacement stage of the anchor. The reason is that with the gradual increase in load, the anchor rod body mainly bears tension, and the load on the anchor rod is transferred to the surrounding mortar body. At this time, cracks begin to appear in the mortal body with the increase in load transfer, and the anchor rod will slip. The second section is the mortar splitting stage. As the load continues to increase, the small cracks that begin to appear in the mortar body gradually increase. With the development of cracks, the bonding force between the bar body and the slurry decreases significantly, resulting in the continuous increase in the slip of the bar body. The last section is the stage of complete loss of bonding force. The interface between mortar and anchor is broken until it is connected, and the anchor body is completely pulled out. Only residual bonding force provided by the friction

force is left at the interface between the anchor and mortar [63].

3.2 Performance of FRP anchors under freeze–thaw cycles

The interaction of the FRP at variable temperatures plays an important role in the long-term durability of FRP. In the freezing-thawing cycle, microcracks and pores may occur due to the mismatch of thermal expansion coefficients of each component element. In tests conducted by Dutta [64,65], from +23 to −40°C, the tensile strength of FRP is reduced by about 10% after 150 freeze-thaw cycles. Saeed *et al.* [66] and Verghese *et al.* [67] investigated the effect of temperature cycling of polymer composite materials in a water bath. They found that although freezing water is nearly impossible in highly cross-linked amorphous polymers such as vinyl esters, the size of the interfacial cracks in the composite system is large enough to facilitate the freezing of water during aging, and the mechanical properties of FRP bars are weakened to some extent after freeze–thaw cycles [68]. The tensile strength of FRP bars decreases from 3.30 to 602.9 MPa, and the elastic modulus decreases from 105 to 29.7 GPa. The elongation at break decreased from 2.6 to 2.2%. The reason for this phenomenon is that the interface between fiber and matrix is destroyed by freeze–thaw cycles. At present, the improvement measures for the decrease in the bonding properties between fibers and the matrix under freeze–thaw cycles are not perfect. One of the methods is surface coating, the purpose of which is to effectively control the absorption and diffusion of water molecules inside the resin matrix. However, with the continuous change in temperature, the coating will swell and bulge, resulting in a decline in its performance. Over time, it will continue to weaken until it fails. Therefore, the improvement measures for this aspect are still in the blank stage so far, and should be supplemented and improved.

3.3 Improved method of FRP anchor

3.3.1 Chemical modification

Chemical modification mainly uses the active groups on the surface of other excellent fibers to stably graft other groups to the surface of fibers through chemical treatment, thereby improving the mechanical properties of the fibers. For example, the composite materials of pure epoxy resin and nano SiO_2 modified epoxy resin prepared by sol–gel method and the coating of epoxy resin/SiO_2 hybrid material are used to modify the FRP. The experimental results show that the hybrid coating formed on the FRP surface increases the roughness of the FRP surface, improves the tensile strength of FRP bars, and further improves the bond between the FRP bars and mortar when the FRP bars are used as an anchor, especially when the SiO_2 content is 5%, the modification effect is the best [69,70]. The presence of two types of nanoparticles improved the surface energy and wettability of FRP, and thus enhanced the compatibility between the fiber and matrix, leading to better mechanical interlock between them.

The torsional strength of the anchor solid increases gradually with the increase in the content of nano-mullite powder (the torsional strength increases by about 35%), but the broken line turns from a rising broken line to a falling broken line when the content of nano-mullite powder is 1.5%, This indicates that the limit of nano-mullite content is 1.5%, which will not increase the torsional strength of FRP anchor but weaken it. The SEM micrograph of FRP anchor solid in Figure 18 can also indirectly verify the trend. As can be seen from the figure, in the absence of nano-mullite powder, the separation interface between the matrix and fiber is used, which will cause the distortion strength of the anchor solid to be in a low state. When the content of mullite powder is 1.5%, a compactness is presented between the matrix and fiber interface, making the torsional strength of the anchored body to be in a high state, and when the content of nano mullite powder is 3.0%, at this time a broken screen is presented between the matrix and fiber, naturally, the anchor solid torsional strength will be in a lower state [71].

The step-by-step method is to place an already crosslinked polymer (first network) into another monomer or prepolymer containing catalyst, crosslinking agent, etc., allow it to swell, and then allow the second monomer or prepolymer in *in situ* polymerization and crosslinking to form a second network, and the resulting product is called a stepwise interpenetrating polymer network (IPN). For example, the chemical structure formed by the polyurethane bond of the acrylic polyurethane emulsion and the ester bond of the unsaturated polyester resin in the matrix phase is an IPN, which has a strong chemical combination tendency and binding force. The chemical IPN structure reduces the penetration range to the nanoscale, thus the combination of the reinforced phase and the matrix phase is dense, and then, the tensile and

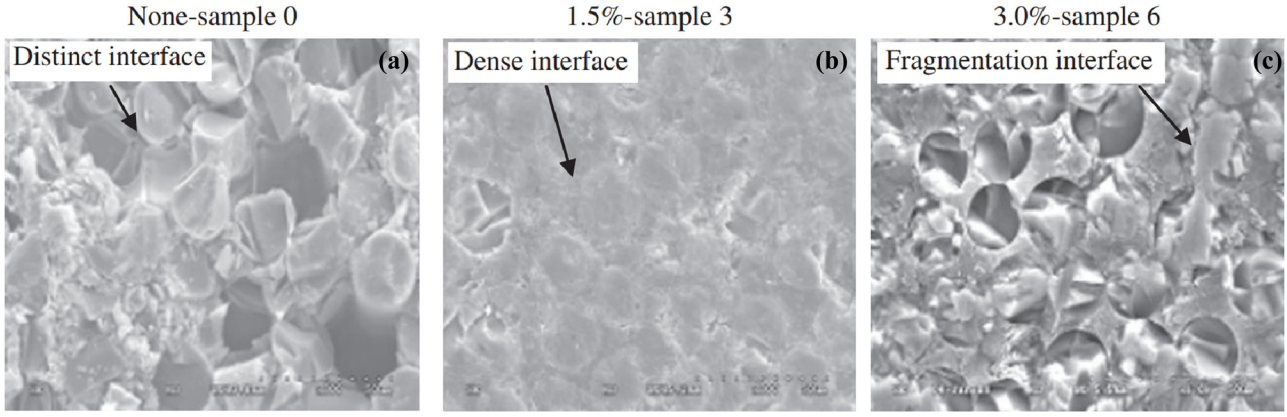

Figure 18: Comparative SEM micrograph of the FRP-anchor body with different nano-mullite contents: (a) none-sample 0, (b) 1.5%-sample 3, and (c) 3.0%-sample 6 [71].

torsional strengths of the FRP-anchor increase [71]. As can be seen from the SEM micrograph of Figure 19, with or without the vacuum pumping process, the interface is very mysterious under vacuum conditions, which will significantly improve the torsional strength of the anchor by about 51% [71]. But there have been no trials of all these three in combination, and this is something that needs to be studied.

The impregnation of fly ash can improve the mechanical properties of FRP bars. First, the tensile performance of FRP anchors is the best when fly ash is not added to FRP anchors and fiber mass ratio is 30% and the polyester mass ratio is 70%. Second, when fly ash is added to the FRP anchor and the fiber mass ratio is 20%, the fly ash mass ratio is 10% and the polyester mass ratio is 70%, the tensile performance of the FRP anchor is the best. Third, after adding fly ash, the tensile strength of the FRP anchor is increased by 10% [72].

Similarly, with the addition of 10% fly ash, the ultimate tensile strength and yield strength of FRP anchors are increased by 5 and 3%, respectively, because fly ash improves the interfacial adhesion between the fiber and matrix. Figure 20 shows the SEM observation on FRP filled with 10 wt% of fly ash indicating that the formation of fiber pullout is arrested, which has led to better stress transfer [73].

In addition, there is a new type of transverse reinforced high-temperature CFRP bar composed of PAN-based carbon fibers impregnated with high-temperature resistant and toughened epoxy resin. Compared with ordinary CFRP bars, the transverse and longitudinal mechanical specific energy gap of the new CFRP bars is narrowed and the transverse compressive strength is 2.5 times that of the common CFRP. Finally, the shear strength of the new CFRP bars is enhanced by 30–40% [74]. Research has shown that modification of epoxy resins with carbon functional silanes and

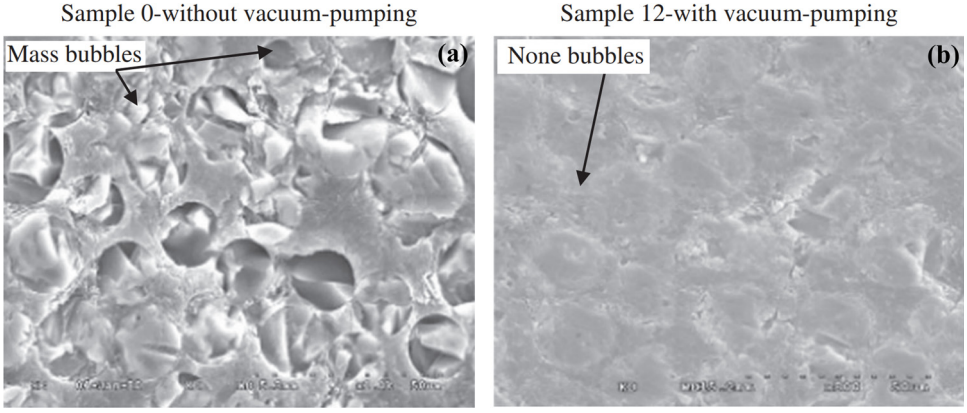

Figure 19: Comparative SEM micrograph of the FRP-anchor body (a) without and (b) with vacuum pumping process [71].

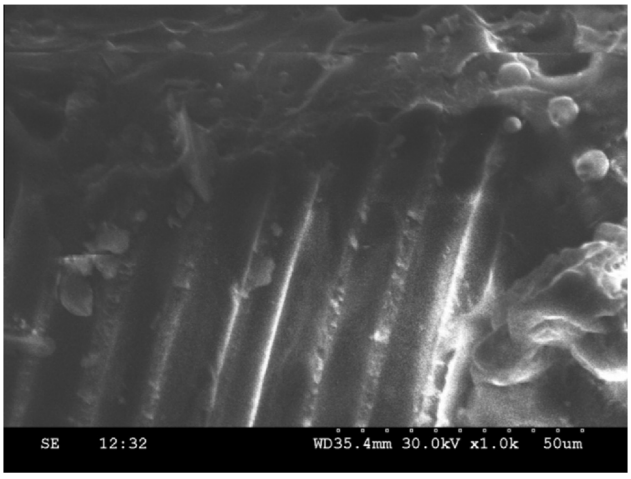

Figure 20: FRP with 10 wt% of fly ash [72].

siloxanes leads to significant improvements in the overall properties of the cross-linked system. Because it has been shown that these materials possess a valuable combination of properties, such as improved mechanical properties, thermal stability, and resistance to oxidation, weathering, and chemicals [75,76]. Applying siloxane and silicon-based coatings to CFRP can reduce the water absorption of CFRP. This can be verified by equation (9) [77].

$$W_{ut} = \frac{P_t - P_0}{P_0} \times 100, \tag{9}$$

where P_t and P_0 are the weights of the specimen at time t and at the initial time, respectively. W_{ut} represents the variation in water uptake over time (W_{ut} represents the change in water absorption over time).

3.3.2 Hybridization with synthetic fibers

Hybrid composites are the complex systems, where the matrix is made up of two or more different materials and two or more different reinforcing or filling materials are embedded in this matrix in order to approach the desired mechanical and processability properties and to reduce the material costs [78]. The properties of FRP reinforcement materials are usually different. For example, BFRP tendons have good alkali resistance but low elongation, while GFRP tendons have high elongation but very low alkali resistance, so if the two fibers are combined, they will compensate for the disadvantages of both the tendons. Fiber blending is a means of quickly achieving the desired mechanical properties of fibers, mainly by blending a variety of fibers to compensate for the deficiencies of each fiber and to make the most of the advantages of each fiber. After the fibers are mixed, the new hybrid fibers will appear pseudo-ductile when they are under tension, which makes up for the defect of brittle failure of pure FRP fiber bars after being stressed. Fracture will occur first, and then the fracture stress will be transferred to the fiber with higher ultimate strain, and it will continue to undergo tensile stress and a ductile stage will occur. Under normal circumstances, the mechanical properties of the mixed fiber tendons are generally between the mechanical properties of the two pure fiber bars. Through experiments, Protchenko and Szmigiera [79] concluded that the hybrid bars have obvious confounding effects, the synergistic performance is better, and the elastic modulus of the bars has been significantly improved. In his literature, the mechanical properties of the hybrid bars after different arrangements were compared in detail and the optimal conclusion was drawn, but no further research was carried out on the fiber content ratio. He *et al.* [80] studied the C/GFRP hybrid bar, studied the arrangement of fibers in the carbon and glass fiber hybrid bar, and found that the mechanical properties of the hybrid bar were the best when the carbon fiber was in the core area of the hybrid bar. However, carbon fiber is not suitable for the manufacture of bolts for two reasons: one is expensive, and the other is that the low elongation of carbon fiber makes the bolts to undergo brittle failure faster, so elongation should be sought in future research. Moderate fibers are mixed with glass fibers to achieve pseudo-ductile effects.

In addition, the tensile strength, elastic modulus, and ultimate strain of the carbon epoxy resin tendons (E-tendons) are 37.8, 5.1, and 27.6% higher than those of the carbon vinyl ester resin tendons (V-tendons). It is similar to carbon E-tendons and basalt E-tendons, the glass E-tendons indicated tensile strength and failure strain that is 3.4 and 9.2% higher than those of the glass V-tendons [81,82].

The hybrid basalt/carbon (B/C) ratio of the V-tendons increased from 1:1 to 2.7:1, 3.6:1, 6.5:1, and 8.2:1 on decreasing the load drop by 66, 79, 86, and 88%, respectively. Additionally, the failure strain and the ductility of B/C tendons are strengthened observably by increasing the high elongation/low elongation fiber volume ratio. Moreover, the failure strain of V-tendons with B/Ce of 8.2:1 is 15% larger than the ultimate strain of the nonhybrid basalt tendons. Furthermore, the ratio of the failure load to the yield load increases nonlinearly with increase in the B/C. Unfortunately, the tendon modulus decreases with increase in the B/C ratio. However, its minimum modulus is still 15% higher than that of the nonhybrid basalt tendon modulus.

4 Corrosion resistance of FRP bars

4.1 Corrosion resistance of FRP bars in alkaline environment

The chemical reaction process of FRP bars in alkali solution is as follows [83]:

$$\text{R–COO–R}^{\cdot} + \text{H–OH} \rightarrow \text{R–COOH} + \text{R}^{\cdot}\text{–OH}. \quad (10)$$

This chemical process mainly means that when water molecules penetrate the resin, the interface bond between fiber and matrix is broken, the resin gap is filled with water, and the free volume of FRP bars is changed, resulting in a large number of cracks in the matrix and hydrolysis reaction.

$$SiO_2 + 2H_2O \rightarrow H_4SiO_4, \quad (11)$$

$$2OH^- + SiO_2 \rightarrow SiO_3^{2-}. \quad (12)$$

The OH^- in water and alkali solution penetrates into the fiber surface through the matrix, resulting in the destruction of the SiO_2 network framework.

$$\text{Si–O–Si} + OH^- \rightarrow \text{Si–O}^- + \text{Si–OH}. \quad (13)$$

With the passage of corrosion time, the interface adhesion between fiber and matrix is weakened, and the interface erosion between fiber and matrix becomes more serious. Moreover, the water molecules and OH^- react with the fibers and continue to destroy SiO_2 network framework, reducing the strength of the FRP bars. There is a lot of OH^- in the alkaline solution, and the silicon–oxygen bond reacts with OH^-, destroying the silicon-oxygen and silane coupling agent.

$$\text{RCOOR}^{\cdot} + \text{NaOH} \rightarrow \text{RCOONa} + \text{R}^{\cdot}\text{OH}. \quad (14)$$

The corrosion of steel anchor is the main reason for the failure of anchorage system structure. In order to solve the corrosion problem of steel bar, domestic scholars think that FRP can replace steel bar after 60 years of research. Although the corrosion resistance of FRP is better than that of steel bar, the mechanical properties of FRP are also damaged with the increase in the duration of corrosion environment. The damage degree of FRP varies greatly in wet, acidic, seawater, and alkaline environments. The mass loss of FRP bars in wet, acidic, seawater, and alkaline environments at high temperature increases gradually with time [84,85]. At the same temperature, the weight gain of the sample immersed in alkaline solution is slightly lower than that of the sample immersed in water [19,86]. And in the four environments, the acid environment causes the most damage to FRP bars. Therefore, a conclusion can be drawn: the alkali resistance of FRP bars is better than acid resistance. Mass loss of FRP in acidic environment is from 4.8 to 5.9% by soaking in different corrosive aqueous solutions at 96°C for 1 and 7 days, but the mass losses are less than 1 wt% after immersion in water, alkaline solution, and saline solution. This leads to the conclusion that FRP is poor acid resistance [87].

However, according to the experimental results of Wu *et al.* [33], alkali resistance of FRP bars is the weakest in the four environments. As can be seen from Figure 21, the comparison of residual tensile strength of FRP bars in different types of solutions shows that the residual tensile strength of FRP bars in the deionized water environment is the largest, followed by the salt solution, acid solution, and alkali solution. Therefore, it can be concluded that the strong retention rate of FRP bars is the maximum in a highly humid environment, while the strength retention rate of FRP bars is the minimum in an alkaline environment. Compared with these four environments, it can be seen intuitively that the alkaline resistance of FRP bars is relatively weak [33]. The difference in the above research conclusions may be mainly due to the difference in the concentration of the solution or the difference in the preparation of the reinforcement material.

In addition, temperature also affects the corrosion rate of FRP in alkali environment, because the higher the temperature, the more strongly the hydroxide ions react with the ions in FRP. It can be seen from Figure 22 that the strong retention rate of FRP bars varies with the temperature in an alkaline environment. It is concluded that with the decrease in temperature, the strength retention rate of FRP bars increases under the same exposure time, and the strength curve of FRP bars shows a very

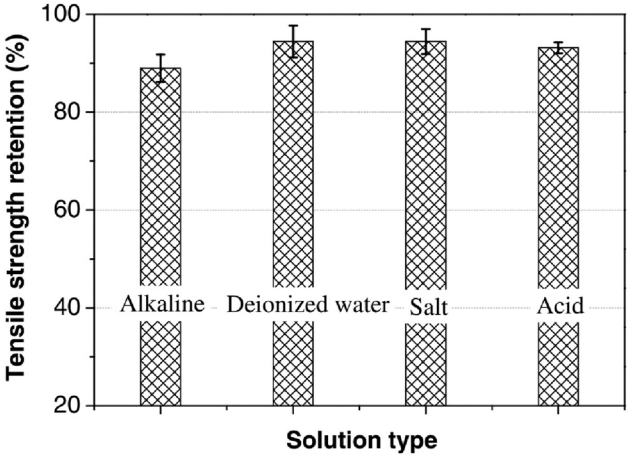

Figure 21: Comparison of residual tensile strength in different types of solutions [33].

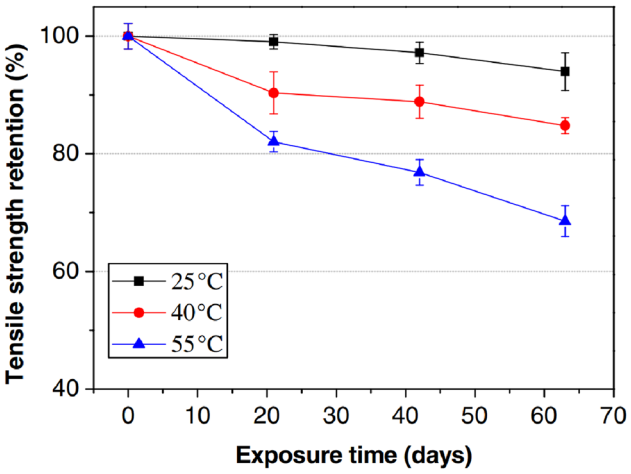

Figure 22: Comparison of strength retention for stress-free bars in alkaline solution at different temperatures [33].

gentle decline under the lower temperatures [33]. In his research, the author focuses on the corrosion mechanism of FRP bars with the increase in time, but the selection of test temperature points is less, and the concentration of temperature distribution is not conducive to seeing some changes in the FRP bars at high temperature. It is recommended to disperse the temperature points for research.

In terms of thermodynamic activity, Mn, Ti, and Fe oxides can improve the alkali resistance of FRP bars. In addition, zirconia coating has a significant slowing effect on the corrosion of FRP bars in alkali solution and the inhibitory effect of dense zirconia coating on the corrosion of FRP bars is better than that of porous coating [88].

4.2 Corrosion resistance of FRP bars in acidic environment

The cause of Al^{3+} dissipation during corrosion of BFRP bars in an acid environment is not clear. One of the hypotheses may be that the consumption of Ca^{2+} and Al^{3+} are two dependent processes, and the large consumption of Ca^{2+} may reduce the stability of GFRP bars and thus promote the consumption of Al^{3+}, which can be used to describe the consumption of Al^{3+} in BFRP bars [89]. The strength and elastic modulus of BFRP bars decreased by 58.5 and 31.5%, respectively, after soaking for 720 h in acid solution, while the strength and elastic modulus of GFRP bars decreased by 44 and 37%, respectively, under the same environment. It can be concluded that the strength of BFRP bars is weakened more than that of GFRP bars in an acidic environment, while the elastic modulus is weakened less than that of GFRP bars [90].

4.3 Corrosion resistance of FRP bars in seawater environment

In the seawater environment, when the FRP bars are placed in seawater solution, the mass of the FRP bars increases rapidly at the beginning, which may be due to the rapid infiltration of some water into the FRP bars and the high void ratio at the fiber–matrix interface. However, some soluble compounds will be extracted with the seawater solution. This causes the mass of FRP bars to decrease, so the curve tends to flatten [91].

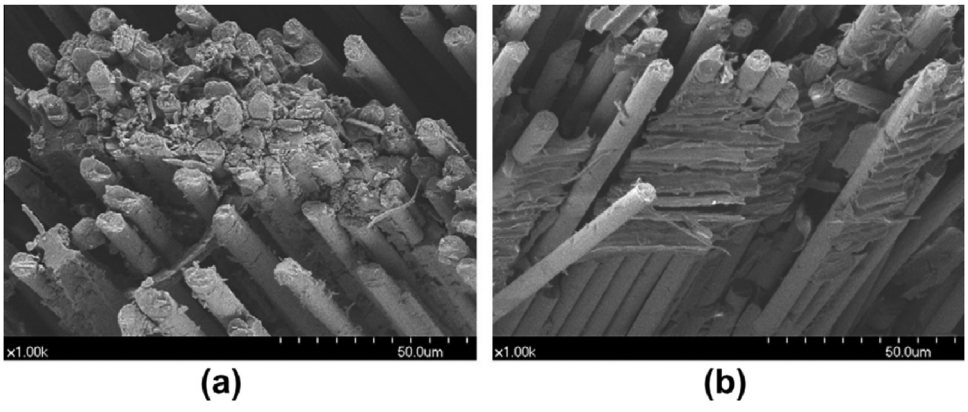

Figure 23: SEM images of the tensile fractures of the BFRP bending specimens: (a) untreated and (b) treated for 90 days [91].

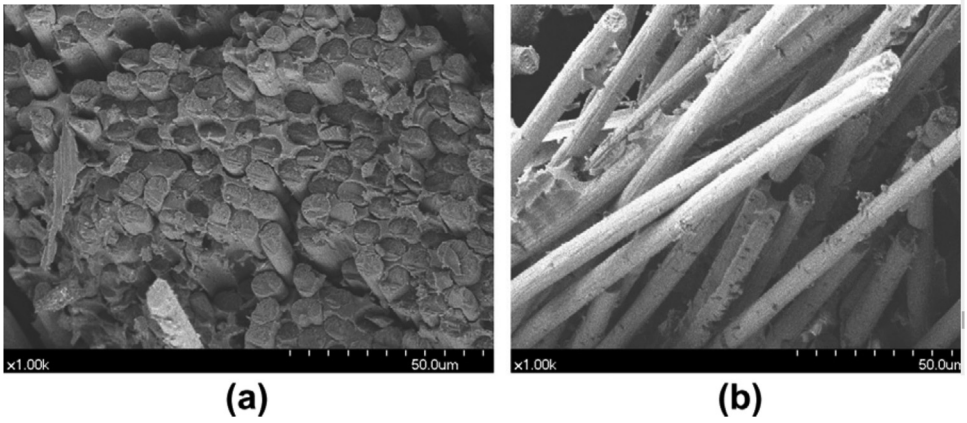

Figure 24: SEM images of the tensile fractures of the GFRP bending specimens: (a) untreated and (b) treated for 90 days [91].

Some scholars have studied the corrosion mechanism of FRP bars by analyzing the corrosion characteristics of FRP bars in seawater by microscopic observation. The comparison between Figures 23 and 24 show that the FRP bars not placed in seawater break neatly after being pulled. This indicates that the adhesion force between the matrix and the fiber interface is good, but after 90 days of seawater corrosion, the adhesion force between the fiber and the matrix is seriously weakened, and the fibers cannot be broken at the same time, and the material will burst into many filaments when damaged [92,93]. The author's article provides a detailed description of the corrosion mechanism of FRP under seawater through microscopic observations, but there is still a gap in the prevention of corrosion. At present, some people in China have developed seawater desalination membrane shells to prevent the corrosion of FRP bars in seawater. This invention is still under continuous research and development. In the research and development of the reliability of the strength of the main card grooves, in the process of research and development of the project, the main research is on the card grooves and coordination between the layers of the fiber layers.

4.4 Microstructure and corrosion analysis of FRP bars

The diffusion/permeability caused by chemical degradation is the main form of corrosion damage of substrate materials, chloride ion around the composite material to the internal diffusion is the main cause of corrosion degradation, the hydrolysis reaction takes place in composite materials, including fiber, matrix, and interface of hydrolysis. Hydrolysis can damage the molecular chain, then reduce the curing degree of crosslinking network, and finally lead to the changes in the performance of FRP tendons [91,94]. However, the matrix type plays an important role in protecting the fibers from corrosion. Some studies have shown that vinyl esters have lower diffusivity but better protection performance than polyester [95]. Some conclusions can also be drawn from the comparison of the internal structure of FRP bars before and after corrosion by SEM in Figure 25. After corrosion, the corrosion area is generally concentrated on the edge of

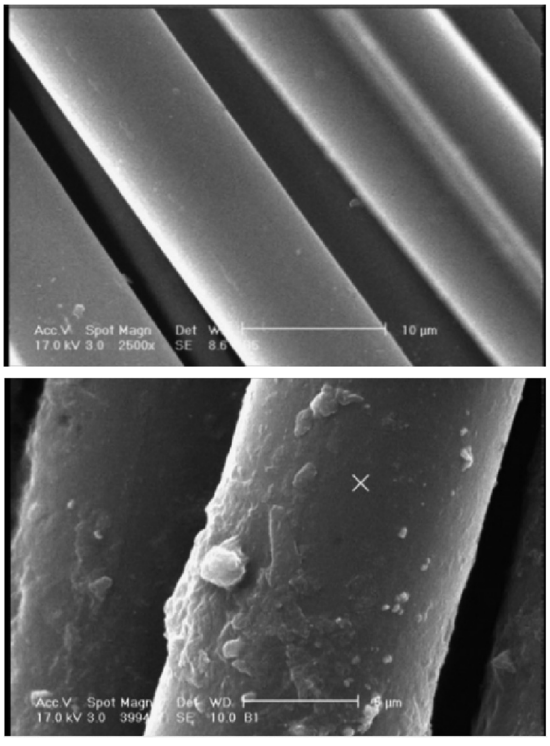

Figure 25: The internal structure of FRP rebar before and after corrosion [90].

FRP bars, and there is almost no erosion inside the bars, which indicates that the erosion of water molecules and OH^- on FRP bars is related to its diffusion path in the FRP bars. Before the corrosion, it can be seen that the fibers and the resin are tightly bonded, and the cracks are hardly visible. The formation of such cracks is initially caused by the erosion of water molecules, but with the increase in temperature, the cracks continue to increase under the joint action of water molecules and OH^-. The fiber degradation is mainly caused by the chemical reaction of water molecules and OH^- with SiO_2 in the FRP bars [90].

The corrosion mechanism of basalt fiber is similar to that of glass fiber. Al^{3+} and Ca^{2+} on the surface of BFRP are leeched out at different soaking times, resulting in the formation of a silicon-rich layer on the fiber surface. However, the strength degradation of GFRP is more serious than that of BFRP, so BFRP can be used as a substitute for GFRP in a corrosive environment [89].

5 Analysis of fatigue resistance and failure mechanism of FRP bars

5.1 Fatigue failure mode of FRP bars

The failure modes of FRP bars are generally divided into four types:

1) "Lantern" failure: fibers and matrix radially diverge from center to periphery along the FRP bar.
2) "Pitting corrosion" failure: failure is only local embedded FRP bar adhesive peeling, fiber, and matrix bare, generally in acidic solution most of this failure form will occur.
3) "Pull crack" failure: longitudinal cracks are running through the FRP bars, and almost all fibers winding outside the matrix are pulled off.
4) "Pull type" failure: FRP bar is completely pulled, generally more such failures occur in the freeze–thaw cycle and acidic environment [96].

Through fatigue tests, Brunbauer and Pinter [97] concluded that the fatigue performance of FRP mainly depends on the bonding between the fiber–matrix interface and the mode of applied load. However, the above literature analysis is not comprehensive enough. Later, scholar Talreja [98] conducted an in-depth discussion. The scholar further found through fatigue loading tests that in general, the stress conditions of FRP composites under fatigue state can be divided into three categories: under high stress level controlled by FRP fiber fracture and under moderate stress by fiber/resin interface The bond strength is determined by the fatigue elongation failure mode at low stress. But there is a problem that the concept of high stress, medium stress, and low stress levels is very vague, and there is no standard numerical limit. Therefore, this gap should be filled in future research. Moreover, the fatigue performance of FRP is relatively complex. At present, there is no unified consensus on the fatigue failure mechanism of FRP, and further in-depth research is still required, such as the fatigue life, fatigue failure mechanism, and fatigue failure model of large-diameter composite materials.

5.2 The fatigue resistance of FRP bars

In general, FRP bars tend to exhibit good fatigue resistance. Tests conducted at the University of Wyoming in Anchorage [99] shows that FRP can withstand 100,000 cyclic loads between 60 and 70% of their ultimate tensile capacity. The fatigue failure of FRP bars is mainly caused by the debonding of the fiber–matrix interface. The fatigue stress range has a great influence on the fatigue life of FRP bars, even at a relatively low-stress level, the cyclic loading stress range also has a great influence on the fatigue life of FRP bars. Demers [100] argues that GFRP composite fatigue data show lower fatigue life for the same normalized maximum stress than the CFRP composite fatigue data. The enhancement of the fatigue resistance of FRP bars can focus on limiting crack propagation and improving the fiber–matrix interface bonding ability, and when FRP bars are used as anchor material, the method of winding fiber anchorage can effectively protect the FRP bars from premature failure in the anchorage zone. Compared with bonding anchorage and friction anchorage, this anchorage method is more suitable for FRP bars in a long-term fatigue environment. Bars can withstand 2 million cycles of load in the stress ranging from $0.05f_u$ (85 MPa) to a maximum stress of $0.6f_u$ (1,018 MPa). Therefore, the recommended stress range of FRP bars in prestressed applications is from $0.04f_u$ (68 MPa) to a maximum stress of $0.53f_u$ (899 MPa) [101].

Due to the low elastic modulus of FRP bars, a large number of transverse microcracks will gradually form in the matrix and gradually diffuse to the fiber–matrix interface with the increase in the number of fatigue load cycles. With the continuous accumulation of transverse microcracks, the fiber–matrix interface will gradually weaken. And due to the shear lag effect of the FRP bars section, the tensile stress on the surface of FRP bars is greater than that of the inner bars, which makes the surface of FRP

bars more prone to fatigue damage. With the increase in cyclic load, the interface debonding between fiber and matrix first occurs on the surface of the tendon, resulting in initial surface rupture. Surface damage spreads along with the peel interface, eventually leading to tendon damage [41]. With the increase in temperature and holding time as the premise, the higher the number of cyclic loads, the more obviously the tensile strength decreases. It can be proved that the increase in the number of cyclic loads accelerates the attenuation of tensile strength of FRP bars at high temperature [35,102].

The average tensile strength of FRP bars is 1,738 MPa and the coefficient of variation is 1.43%, which indicates that FRP bars have potential applicability as prestressed bars. Figure 26 shows the failure of BFRP bars under short-term failure load. No failure is observed at the anchor zone. The results of the short-term tensile test are shown in Table 1. The high ultimate strength (1,719 MPa) and low coefficient of variation (CV) equal to 3.25% show the feasibility of BFRP tendons for prestressing applications [103].

Fatigue prediction:

1) Whitney's method is based on two assumptions: a classic power law representation of the S-N, and a two-parameter Weibull distribution of cycles-to-failure as shown by the following:

Figure 26: Failure mode in the short-term tensile test [103].

Table 1: Short-term tensile properties (data from ref. [103])

Specimen number	Tensile capacity (kN)	Tensile strength (MPa)	Elastic modulus (GPa)	Fracture (%)
BE-1	48.7	1,784	53.9	3.31
BE-2	45.7	1,674	53.7	3.12
BE-3	45.0	1,648	54.0	3.05
BE-4	46.6	1,707	53.4	3.20
BE-5	48.7	1,784	53.3	3.25
Mean value	46.9	1,719	53.7	3.20
CV	3.25%	3.25%	0.51%	3.48%
95% guaranteed strength	44.4		1,628	

$$P_S(N_i) = \exp[-(N_i/\overline{N_l})]^{\partial f_i}, \tag{15}$$

where N_i is the cycle number under the ith stress level; $\overline{N_l}$ and a f_i is the scale and shape parameters of the Weibull distribution under the ith stress level, respectively; and $P_s(N_i)$ is the probability of survival after N_i cycles.

2) Practical infrastructures are exposed to different aging temperatures. Thus, the prediction of the fatigue strength degradation of BFRP tendons at different temperatures is necessary. This prediction is based on the Arrhenius equation, as expressed as follows:

$$K = A\exp(-E_a/RT - \ln A), \tag{16}$$

where k is the degradation rate; A is the constant related to the material and degradation process; E_a is the activation energy; R is the gas constant; and K and T are absolute temperatures.

Generally, for calculation convenience, the above Arrhenius equation can be transformed into equation (17) as follows:

$$\ln(1/k) = E_a/RT - \ln A. \tag{17}$$

Suitable conditions: The prediction using the Arrhenius equation is based on the assumption that a single dominant degradation mechanism exists with different aging temperatures and durations.

To adopt the Arrhenius equation to predict the fatigue strength at different temperatures, the degradation of the fatigue strength concerning aging duration should be clarified. The degradation formula of the most commonly used is the Bank's formulation given as follows [104]:

$$10^{\gamma} \propto \frac{1}{kt}, \tag{18}$$

where γ is the ratio of residual fatigue strength to the ultimate tensile strength; and t is the aging duration.

By substituting the Arrhenius equation in equation (18), it is deduced that

$$10^{\gamma} \propto -\ln(t) + \frac{1}{T}. \tag{19}$$

Thus, the degradation formula at a certain temperature is expressed as follows:

$$\gamma = a_1 - b_1 \ln(t), \tag{20}$$

where a_1 and b_1 are the regression constants; and t is the service duration in days.

6 Application and improvement of FRP bars as slope support

6.1 Application status of FRP anchor

Anchoring technology in geotechnical engineering is to reinforce rock and soil body with anchor rod or anchor cable, which can give full play to the stability of rock and soil body itself. It is a safe, reliable, and economic means of strengthening rock with little disturbance and fast construction speed. The development and application of anchorage technology is an important symbol of modern geotechnical engineering. At present, the development of anchorage technology is in the period of unfolding. The study of anchorage theory is very important to promote the development of geotechnical engineering. The anchor used in geotechnical engineering is a kind of set deep in the rock and soil layer stress bar, its one end connected to the engineering building, the other end of the anchor in rock and soil layer, the prestressing when necessary to soil pressure, water under pressure or tension produced by wind load, which effectively structure under load, to prevent the deformation of structure, so as to maintain the stability of the structure. For a long time, there are durability problems caused by steel corrosion in the rock-soil anchorage structure with steel anchor, and the corrosion occurs in the free section of steel anchorage and the exposed part of anchor head. Passive anticorrosive measures not only increase the cost of the project, but are also difficult in solving the problem fundamentally. Therefore, in order to overcome these defects, a new FRP anchor is used instead. FRP bars are widely used to make anchor because of their high tensile strength, excellent corrosion resistance, and good deformation coordination with rock [69,105,106]. Ultimate bearing capacity of FRP anchor (without considering environmental factors) is as follows:

$$T_{\mathrm{u}} \begin{cases} \Pi dl\psi\tau_{\mathrm{g}} (l_{\mathrm{cr}} < l \le l_{\max}) \\ \Pi f_{\mathrm{g}} d^2/4 (l > l_{\max}), \end{cases} \tag{21}$$

where T_{u} is the anchorage force; l is the length of the anchor; τ_{g} is the bond strength between the anchor and slurry; d is the diameter of the anchor; and Ψ is the effective factor of anchorage length.

6.2 Failure type and failure mechanism

6.2.1 FRP anchor tensile failure

Failure modes of FRP anchor anchorage joint rock mass can be divided into three types. The FRP anchor is pulled apart, shear failure between the FRP anchor and mortar (first interface failure), and shear failure occurs between the mortar and surrounding rock (second interface failure). In the first interface damage, FRP anchors are mainly subjected to external tension, the bonding force between the rod and the slurry. When the external force is less than the bonding force between the rod and the slurry, the FRP anchor does not slip. When the external force breaks through the maximum bonding force, the rod slips with the increase in the external force and is eventually pulled out completely, with a small amount of slurry adhering to the rod after extraction. This is mainly due to the insufficient bond between the slurry and the rod, and the failure mechanism is also due to the fact that the bond between the slurry and the rod < the external force on the rod < the bond between the slurry and the soil.

In the second interface damage, it happens that the rod and the slurry are pulled out together as a whole. The premise for this damage to occur in the first place is that the bonding force between the slurry and the rod must be greater than the external force on the rod, so that the rod and the slurry can be considered as a whole. The bond-slip behavior is such that when the external force is less than the bonding force between the slurry and the soil, the rod and slurry as a whole do not slip, but when the external force exceeds the maximum bonding force between the slurry and the soil, the rod and slurry as a whole will slip. As the external force increases, the rod and pulp are eventually pulled out. The failure mechanism is mainly due to the maximum bond between the slurry and the soil < external force < bond between the slurry and the rod.

The failure point is generally in the free section of the anchor when it is broken. In practical engineering, it is expected that the failure of the anchor body will occur, because such a case can indicate that the anchorage strength

between the anchor body and the mortar body is fully exerted, and it is considered that increasing the anchorage length and the strength of the mortar will not continue to improve the anchorage performance of the anchorage system [107].

6.2.2 First interface damage and preventive measures

With the increase in load, the pulling force is greater than the bonding force between the anchor rod body and the anchor mortar, which will cause cracks between the anchor body and the mortar, resulting in weakened bite force and adhesive force. When the pulling force continues to increase, the rod body will be pulled out or the fibers will be pulled out [62,108,109].

The main characteristics of the first interface failure are that in the process of drawing, the sound of "boom" is constantly emitted from the mouth of the rock mass, showing the law from the surface to the interior, from shallow to deep. This is caused by the gradual weakening of the bond force between the anchor body and slurry under the action of tensile force. The results show that there is obvious interfacial shear at the first interface, and the tension splitting phenomenon of slurry indicates that there is a dilatancy phenomenon at the anchorage interface.

In general, the average bonding strength of the first interface is used to describe the bonding strength of the first interface [110] as follows:

$$\tau_1 = \frac{P_{\max}}{\Pi l d}, \tag{22}$$

where $P_{\max}$ is the pull-out force when the anchor is broken; τ_1 is the average bonding strength of the first interface; d is the anchor diameter; and l is interfacial bonding strength.

Initial stiffness (k_i) is the slope of the load–slip curve at the loaded end from the original point and is expressed as follows [111]:

$$K_i = \frac{T}{\delta}. \tag{23}$$

The concept of average bonding strength is also introduced to allow people to more intuitively calculate the respective bonding strength of the first interface and the second interface, to better predict the damage of the first interface and the second interface under the drawing load in advance. The allowable bonding strength between FRP anchor and mortar = Average pull bond strength ÷ 2.1. The allowable bond strength safety factor is 2.1. There are two reasons for the low adhesion between the FRP anchor and mortar. FRP anchor is anisotropic and coated with a smooth resin layer, which reduces the surface friction between the anchor and mortar. The resin layer has poor shear and compressive properties and is easily broken by shear or dilatation [112].

The first method to improve the bonding strength of the first interface is to increase the amount of sand in the slurry. This method can not only increase the friction between the rod and the slurry, to improve the bonding force of the first interface, but also improve the anti-splitting ability of the grouting body, resist the dilatancy effect, and increase the binding force on the anchor. The bonding strength between FRP anchor and neat cement grout is 2.24–3.01 MPa, and between FRP anchor and mortar is 4.77–12.23 MPa [113]. In general anchoring engineering, it is recommended to use mortar with a strength grade of M15, and high strength mortar can be used in special anchoring engineering [107]. When the compressive strength of anchorage mortar is 41.5 and 55.5 MPa, the average bonding strength between FRP anchor and mortar is 6.43 and 10.47 MPa, respectively.

Second, the diameter of the FRP anchor should be properly reduced so that the anchor and slurry can be integrated more completely. Figure 27 shows that when other conditions remain unchanged, with the increase in diameter, the average bonding strength of the anchor body gradually decreases to 10.47, 8.66, and 7.11 MPa, respectively. This is because the increase in the contact area between the rod and mortar is greater than the increase in the drawing capacity with the increase in the rod diameter [114].

Third is to make the surface of the FRP anchor rough to increase the gripping force of the slurry. The last method is to reduce the bonding length of the anchor appropriately. As can be seen from Figure 28, when other conditions remain unchanged, the bond strength of the FRP anchor interface increases with the decrease in bond length of the anchor [111,113,115].

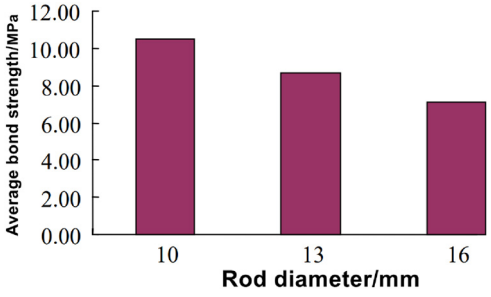

Figure 27: Histogram of average bond strength–diameter [42].

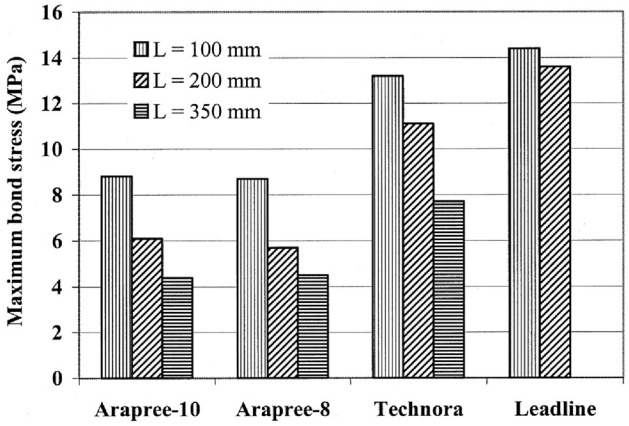

Figure 28: Maximum bond stress of different FRP rods grouted with different bonded lengths [111].

6.2.3 Second interface damage and preventive measures

The main feature of the second interface failure is not the sustained sound of the anchor during drawing like the first interface failure, but a loud "bang" from the depth of the anchor when the anchor system reaches the ultimate bearing capacity. After the anchor is removed, it is found that the grouting fracture instantly produces a slip of nearly 20 cm. It is easy to see that the displacement of the anchorage system changes greatly when it reaches the ultimate tensile force [112].

The average bonding strength of the second interface is expressed as follows:

$$\tau_2 = \frac{P_{\max}}{\Pi l D}, \tag{24}$$

where D is the hole diameter; and τ_2 is the average bonding strength of the second interface.

The degree of weathering has a great influence on the bonding strength of mortar and surrounding rock. The higher the weathering degree is, the greater the influence is on the bonding strength. The diameter of the borehole also affects the bonding strength of surrounding rock and mortar. The smaller the diameter is, the smaller the bonding strength is ref. [81]. By adding an expansion agent to the slurry, the main mechanism is to form a negative Poisson's ratio, so that the diameter of the anchor body becomes larger when the anchor is under tension, which is contrary to the traditional conclusion, so as to better improve the anchoring performance. The excavated FRP anchor grouting has good integrity. However, after dissecting the anchor solid, it can be seen that the surface of the FRP anchor with an anchor length of 2 m has an obvious chafing phenomenon, and the top of the transverse rib is white, which is formed by the friction of the resin layer on the surface. The interface wear of grouting is also serious, white mortar powder remains on the interface, and the first interface may be damaged earlier than the second interface when the rock mass performance is better. Therefore, it is concluded that the first interface of the FRP anchor should be further discussed [112,116,117].

6.3 Effect of anchor on slope reinforcement under earthquake action

6.3.1 Earthquake damage of slope without support

The seismic damage of the unsupported slope mainly occurs at the top of the slope and the surface of the slope, and the development process of displacement failure is the occurrence of tensile cracks at the top of the slope. Shear cracks appear on the air surface → fracture extension → slope subsidence and soil peeling occurred at the cross position of cracks → the shallow surface of the slope is stratified from top to bottom. Seismic action on an unsupported slope can cause significant displacement of the slope. For example, when the peak value of the input wave is 0.2 and 0.4 g, the displacement of left slopes (unsupported slope) has a sudden change. The reason is that under the action of a 0.2 g seismic wave, the slope changes from elastic stage to plastic stage, and under the action of a 0.4 g seismic wave, the slope sliding surface is formed. As the cumulative damage inside the slope increased, cracks gradually increased (consumption of seismic energy) and the filtering effect becomes more and more intensified. At the stage of plastic strengthening, the amplitude of the dynamic stress intensity factor of rock mass increases to its fracture toughness, resulting in a sharp decrease in the number of microscopic cracks and a significant increase in the damage rate until failure [118].

6.3.2 Effect of FRP anchor on slope reinforcement under earthquake action

The FRP anchor has high tensile strength and low elastic modulus, and within a certain range, it can produce synergistic deformation with the slope. In the condition of 8 (seismic peak acceleration of 0.8 g, mesa of input waveform for EI wave,) for the x direction contrast under the condition of the left picture (steel anchor reinforced slope), the right picture (FRP anchor reinforcement slope) can see the left picture near the sliding zone of slope body

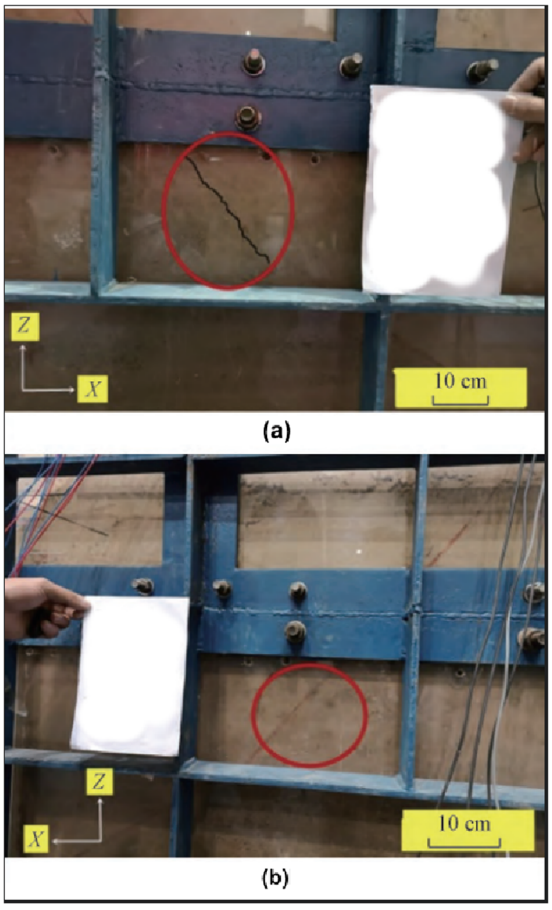

Figure 29: Deformation of slope under action of working condition 8: (a) left oblique fracture and (b) no fracture was observed on the right side [119].

position in the oblique cracks, and the picture on the right slope sliding zone near the position not seen obvious cracks [119], which was shown in Figure 29.

Figure 30 shows the displacement spectrum distribution of each measuring point on the slope breaking surface without support. Figure 31 shows the displacement spectrum distribution of each measuring point on the slope surface of the FRP anchor support side, $N_1 \rightarrow N_7$, $A_1 \rightarrow A_7$ is the measuring point from bottom to the top of the slope. Under the action of the low earthquake, the displacement of left and right amplitudes is less than 1.3 cm, the displacement is very small. It can be considered that the left and right slopes are inelastically stated under the condition of the low earthquake. It can be seen from the figure that the displacement at the top of the slope is larger than that at other slope positions, with displacement values of 1.86 and 1.66 cm. By comparing the two figures, it can be seen that the displacement of the slope supported by FRP anchor is much smaller than that of the slope without support. It can be shown that an FRP anchor can indeed limit the slope displacement well [120].

The above article only compares and studies the displacement under different anchors. Under the action of earthquake, it is also necessary to analyze the displacement of different parts of the slope in order to intuitively analyze which part of the slope has the greatest impact on the internal force of the earthquake, which can also be used for reference in future prevention. For instance, Figure 32 shows the survey pipe located at the leading edge of the slope toe, and the survey pipe is located in the FRP anchor test area. And Figure 33 shows the survey pipe at the top of the slope, also in the FRP anchor test area. It can be seen that the maximum deformation of the slope foot of the FRP anchor test area is 1.2–2.2 mm, and the maximum deformation of the slope top of FRP anchor test area is about 5.0 mm. Therefore, anchorage research should be conducted on the slope top in the future.

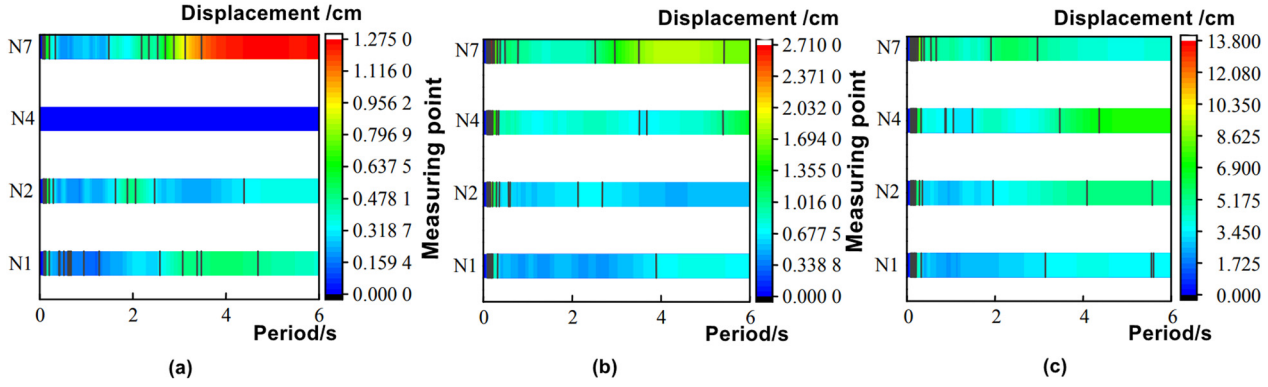

Figure 30: Displacement spectrum of each measuring point on the left slope: (a) downslope position shift spectrum under low shock, (b) downslope position shift spectrum of medium earthquake action, and (c) downslope position shift spectrum of strong earthquake [120].

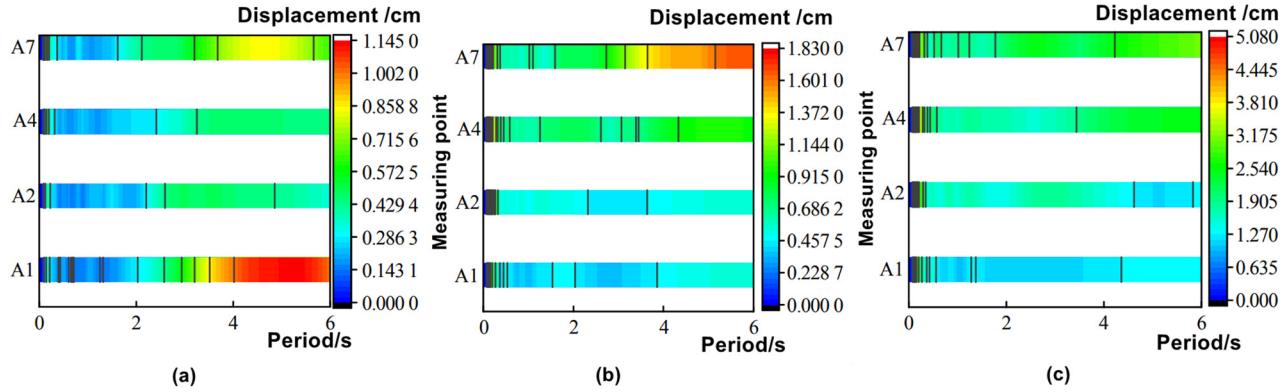

Figure 31: Displacement spectrum of each measuring point on the right slope: (a) downslope position shift spectrum under low shock, (b) downslope position shift spectrum of medium earthquake action, and (c) downslope position shift spectrum of strong earthquake [120].

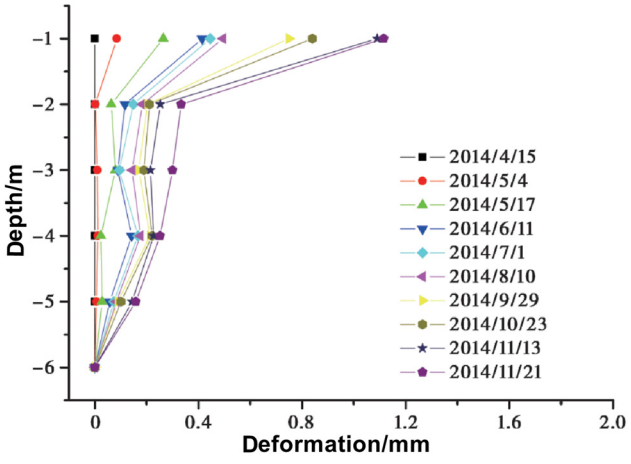

Figure 32: Deformation curve of the inclined tube of No. 3 [48].

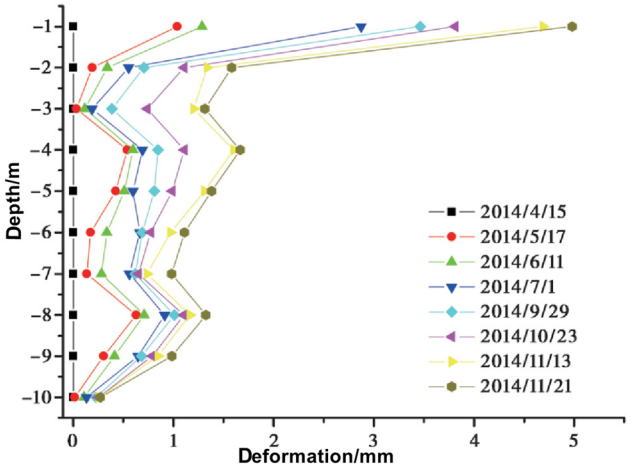

Figure 33: Deformation curve of the inclined tube of No. 6 [48].

6.4 Finite element analysis

6.4.1 Comparison of results of field anchoring by simulation

Finite element software is widely used in slope simulation. It can be seen from the monitoring results of the slope displacement strengthened with FRP anchors in Figure 34 that the slope displacement within 6 m underground is increased after the excavation of the secondary slope on May 5, but the deformation rate decreased after the reinforcement with FRP anchors. Therefore, it can be concluded that the FRP anchors can effectively control the slope displacement [41]. Compared with Figure 35,

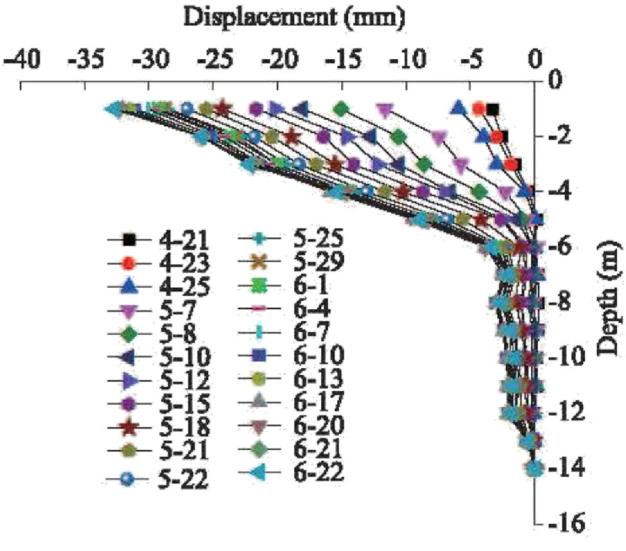

Figure 34: Displacement curves of CX6 in slope supported by FRP anchor [41].

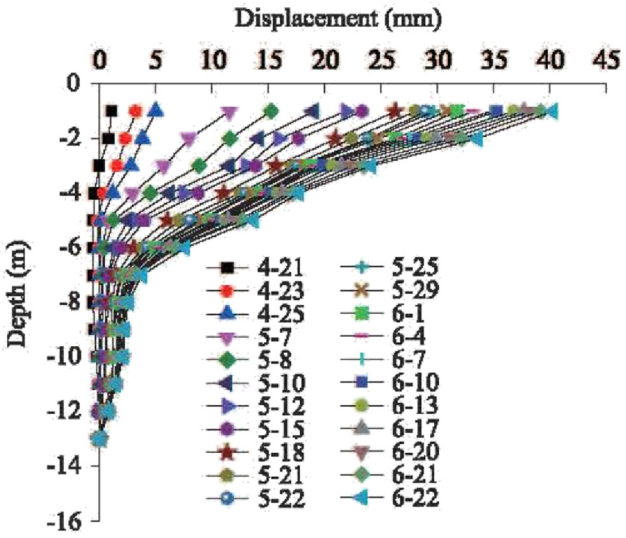

Figure 35: Displacement curves of CX7 in slope supported by steel bar anchor [41].

it can be seen that the slope displacement of the steel anchor is the same as that of the FRP anchor. However, by June 22, the slope displacement of the steel anchor is 41 mm larger than that of the FRP anchor, so it can be seen that the slope displacement of the FRP anchor is better than that of the steel anchor.

6.4.2 Load–displacement simulation curve of the FRP anchor

In the normal test, the complete load–displacement curve of FRP without failure anchor cannot be obtained, which is a lack of substantive reference for practical engineering. Therefore, it is necessary to use the function model to describe the prediction of the ultimate tensile capacity of the anchor that fails to be loaded to the failure state. The common models are the hyperbolic function model, exponential function model, power function model, and exponent-power function model. The fitting curve form of the finger-power function model is very similar to that of the exponential function model, and the prediction accuracy of the finger-power function model for ultimate tensile capacity is less than 1% [108].

Many scholars at home and abroad also use the two-parameter Weibull statistical model to describe the failure curve of FRP anchor tensile strength. The theoretical basis is that the Weibull strength theory has a strong similarity with the tensile failure mode of FRP composite. The basic form of the Weibull distribution function is as follows:

$$P(\sigma) = 1 - \exp\left(-\left(\frac{\sigma}{\eta}\right)^{\beta}\right), \tag{25}$$

where σ is the tensile strength of the FRP anchor; $P(\sigma)$ is the cumulative failure probability; η is the scale parameter; and β is the shape parameter.

7 Biological polymer

7.1 Composition and form of natural fibers

Natural fiber is a broad term which can be divided into vegetable and animal fibers. First, the main component in plant fibers is cellulose, so plant fibers, also known as natural cellulose fibers, are fibers obtained from seeds, fruits, stems, leaves etc., of plants. Depending on the part of the plant where it grows, it is divided into seed fibers, leaf fibers, and stem fibers. For example, olive leaves contain 11.28% cellulose, 14.73% hemicellulose, 16.33% lignin, and 57.66% others. First, the surface roughness of the olive fibers provides mechanical interlocking in the composite and thus a good interfacial bond between the olive fibers and the matrix. Experimentally it can be concluded that as the fiber load increases, the fibers increase the flexural modulus of the composite, which is determined by the increase in the fiber content, and that the fibers have sufficient stiffness over the matrix. Olive fibers enhance the flexural properties of green composites when used to produce low-cost green materials. This is why olive fibers will be useful in the future for biological products where bending resistance is required.

7.2 Added value of biological additives in strengthening polymers

Natural fibers are commonly used to improve the mechanical properties of polymer matrices and to obtain new desired properties in reinforced polymer composites. In addition to environmental friendliness and low cost, natural fiber also has the advantages of greater stiffness, strength, fatigue strength, corrosion resistance, impact absorption ability, and so on. So, when natural fibers are added to the biological products produced in manufacturing, they can improve the mechanical and physical properties of the biological products. For example, olive fiber can enhance the flexural performance of low-density

polyethylene. When the fiber volume fraction reaches 40%, the maximum flexural strength reaches 34.6 MPa, and the bending modulus is greater than 800 MPa [121]. In addition, nanofibers also have great advantages. First, their diameter is less than 100 nm, and their large surface area per unit mass provides the unique ability to adsorb or release absorbing molecules, functional groups, catalytic groups, and several types of nanoscale units. The addition of nanofibers also provides great adhesion ability to nanocomposites and increases the intermolecular binding, which promotes the mechanical properties of nanocomposites to be greatly improved.

The microscopic analysis of nanocomposites is summarized in the above literature in great detail and is of great significance. However, it is suggested that the microscopic experiment and simulation of nanocomposite materials should be supplemented in the future, so as to better understand and explore this material by combining micro and macro. Subsequently, AL-Oqla *et al.* [122] proposed that the interface bonding between the components of the biological composite material is the key to control its mechanical properties, and verified it through impact resistance experiment and tensile test. Thus, the most constructive reinforcement conditions to reduce the internal damage of the composite materials are analyzed more intuitively. A final mention is made of palm sugar fiber, which is known for its own durability and water resistance. It is currently used as a reinforcing agent in polymer-based composites. When polyvinylidene fluoride is reinforced with palm fibers, a series of tests including tensile, flexural, and nano-mechanical tests can be carried out to conclude that their mechanical and physical properties make them an excellent material for outdoor and light applications. The main contributions of palm fibers are strength, stiffness, and Young's modulus and the reinforced composite has excellent resistance to water absorption and thickness expansion. This makes the composite material more suitable for photovoltaic backsheets, interior components for the automotive industry, decorative design, outdoor products, and ecodesign products.

7.3 Advanced selection processes and methods for bio additives in composites

Biopolymers are natural polymers produced by living organisms. In other words, they are polymerized biomolecules derived from cells or extracellular material. The main difference between biopolymers and synthetic polymers is their structure. All polymers are made of repeating units called monomers. Biopolymers usually have well-defined structures. In contrast, most synthetic polymers have simpler, more random structures.

At present, the advanced selection process and method of biological additives are of concern for scholars at home and abroad. Natural fiber materials are limited by some constraints and factors in specific industrial sectors, and the selection of suitable natural fiber types is influenced by many criteria, which is considered as a multi-criteria decision making question [123]. Therefore, choosing the most appropriate type of material for a particular application is a complex issue that requires proper evaluation and decision making. The existing selection methods are sample additive weighted method, the analytic hierarchy process, Fuzzy-AHP technique, graph theory, Vise kriterijumska Optimizacija kompromisno Resenje method, weighted product method, as well as others. For example, the AHP model can be optimized to find the most suitable, cheapest, and most environmentally friendly alternative materials, which can not only improve the sustainability and productivity of the automotive industry, but also improve the environmental performance.

In the proposed combined multi-criteria evaluation stage technique, the criteria affecting the proper selection of natural agro waste fibers were combined together and divided into categories or stages as follows: single-evaluation-criterion, combined-double-evaluation-criterion, combined-triple-evaluation-criterion, etc. Comparisons only up to combined-triple-evaluation-criterion were demonstrated because results became more obvious with increasing combinations. The suggested combined evaluation criteria were proposed based on single physical, single economic, and single mechanical evaluation criteria for the first category. Combined physical-mechanical criteria were utilized in the second category, whereas combined physical-mechanical-economic evaluation criteria were implemented in the third category to achieve better, more consistent, and more informative selection decisions. To illustrate the effectiveness of the proposed technique in evaluating agro waste fibers for natural fiber reinforced polymer composites, pairwise comparisons between six different natural fiber types were simultaneously performed for each proposed category. Each comparison with respect to each single proposed stage is interpreted in a separate illustration.

7.4 New generation biopolymers and the properties of bioproducts

A new generation of biopolymers is now slowly becoming known, such as active polymers. This polymer, which

often responds to stimuli such as electric and magnetic fields, pH, and light, can significantly broaden the range of applications for a wider range of biological products. One notable application of active polymers in the new generation of biopolymers is found in bionics, including artificial vision, artificial intelligence, artificial muscles, etc. This development is limited by complex drives, dynamics, and controls that are unmatched by simple natural systems. There are also a number of potential applications in energy harvesting, robotics, green technology, energy storage components, dielectric elastomers, solar cells, and biosensors.

Over the last 20 years, advances in PV technology have flourished thanks to valuable discoveries. Improvements in PV backsheet structures and their optical performance enhancements have yielded great results in optimizing solar radiation, reflectivity, and PV cell performance. A number of researchers are currently investigating the issue of replacing conventional photovoltaic backsheets, and the material of choice is a new generation of biopolymers – polyvinylidene fluoride. Polyvinylidene fluoride has good resistance to sunlight degradation and high solar transmittance. The combination of this polymer with short sugar palm fibers from natural fibers has resulted in a new generation of photovoltaic backsheets, which have been electrically and thermally evaluated to conclude that vinylidene fluoride short sugar palm fiber backsheets have proven to be thermally stable, exhibiting less energy absorption, and better temperature variation. The optical properties of the material were further investigated by a number of researchers in addition to electrical and thermal tests, and Fourier transform infrared spectroscopy showed the presence of a specific chemical composition in the composite. The absorbance and transmissivity have good stability.

8 Conclusion

This review mainly introduced the mechanical properties of FRP, including tensile and fatigue properties, and also focus on the current research progress and innovation of FRP anchor in anchorage engineering, to provide a basis for the design of FRP anchor. In this study, the failure characteristics and the problem of insufficient bonding strength of the first interface (the interface of FRP anchor and mortar) of FRP anchor anchoring slope were discussed, and the improvement was introduced. This review will be conducive to the extension and application of FRP composites as the structural materials in civil engineering. In addition, there is some crucial reference significance and value for the development of a green and sustainable engineering structure. The conclusions are as follows:

1) At present, there is little information on the use of expansion grouting as filler material in bonded FRP anchorage systems, and more research should be done. And there is no scholarly determination of the optimum content of expansion agent in expansion anchors, which should be refined in future tests for this aspect.
2) Since the relationship between the elastic modulus of FRP bars and the diameter of FRP bars still have different views, further tests are needed to confirm and unify the relationship. Similarly, there is no unified conclusion on the comparison between acid and alkali resistance of FRP bars.
3) In an acidic environment, the causes of Al^{3+} dissipation in the corrosion process of BFRP bars is not clear, so it is necessary to do more tests of BFRP bars in an acidic environment, and then analyze the final cause of Al^{3+} dissipation from the SEM diagram. And the domestic FRP bar corrosion test is mostly some macroscopic mechanical test, it is suggested to study from both macro- and micro-aspects.
4) To make FRP anchors more suitable for seismic applications, more cyclic tests should be done to determine the strength weakening range of FRP anchors under seismic applications. It is suggested that the performance of FRP anchor in the freezing–thawing cycle should be further studied in the future.
5) The properties of FRP fibers have been extensively researched and there has been a trend towards hybrid fiber anchors. In the future, two aspects of this area should be investigated in detail, the first being the type and arrangement of hybrid fibers and the second being the optimum range of volume content ratios for two or more fibers.
6) The fatigue properties of FRP are complex, and there is no unified consensus on the fatigue damage mechanism of FRP, and further in-depth research is needed, such as fatigue life, fatigue damage mechanism, and fatigue damage models for large diameter composites.

Acknowledgments: The research in this paper has been supported by the National Natural Science Foundation of China (Grant No. 51708092) and China Postdoctoral Science Fund Project (Grant No. 2018M631894).

Funding information: National Natural Science Foundation of China (Grant No. 51708092) and China Postdoctoral Science Fund Project (Grant No. 2018M631894).

Author contributions: All authors have accepted responsibility for the entire content of this manuscript and approved its submission.

Conflict of interest: The authors state no conflict of interest.

References

[1] Saxena, M., A. Pappu, A. Sharma, R. Haque, and S. Wankhede. Composite materials from natural resources: Recent trends and future potentials. In *Advances in Composite Materials*, Woodhead Publishing, Cambridge, 2011.

[2] Barone, J. Polyethylene/keratin fiber composites with varying polyethylene crystallinity. *Composites Part A Applied Science Manufacturing*, Vol. 36, No. 11, 2005, pp. 1518–1524.

[3] Jawaid, M., H. P. S. A. Khalil, A. Abu Bakar, and P. N. Khanam. Chemical resistance, void content and tensile properties of oil palm/jute fibre reinforced polymer hybrid composites. *Materials & Design*, Vol. 32, No. 2, 2011, pp. 1014–1019.

[4] Ganesan, C. and P. S. Joanna. Fatigue life and residual strength prediction of GFRP composites: An experimental and theoretical approach. *Latin American Journal of Solids Structures*, Vol. 15, No. 7, 2018, id. 16.

[5] Feng, P., J. Wang, Y. Tian, D. Loughery, and Y. Wang. Mechanical behavior and design of FRP structural members at high and low service temperatures. *Journal of Composites for Construction*, Vol. 20, No. 5, 2016, id. 11.

[6] King, R. Fibre-reinforced composites materials, manufacturing and design. *Composites Part A Applied Science Manufacturing*, Vol. 20, No. 2, 1989, pp. 172–173.

[7] Deak, T. and T. Czigany. Chemical composition and mechanical properties of basalt and glass fibers: A comparison. *Textile Research Journal*, Vol. 79, No. 7, 2015, pp. 645–651.

[8] Wu, Z., X. Wang, K. Iwashita, T. Sasaki, and Y. Hamaguchi. Tensile fatigue behaviour of FRP and hybrid FRP sheets. *Composites Part B Engineering*, Vol. 41, No. 5, 2010, pp. 396–402.

[9] Fiore, V., G. Di Bella, and A. Valenza. Glass–basalt/epoxy hybrid composites for marine applications. *Materials & Design*, Vol. 32, No. 4, 2011, pp. 2091–2099.

[10] Wu, Z., X. Wang, and G. Wu. Advancement of structural safety and sustainability with basalt fiber reinforced polymers. *CICE*, Vol. 1, 2012, pp. 1–29.

[11] El-Hacha, R. Prestressing concrete structures with FRP tendons (ACI 440.4R-04). In *Structures Congress*, ASCE, Reston, 2005, pp. 20–24.

[12] Bhat, T., V. Chevali, X. Liu, S. Feih, and A. P. Mouritz. Fire structural resistance of basalt fibre composite. *Composites Part A: Applied Science and Manufacturing*, Vol. 71, 2015, pp. 107–115.

[13] Mingchao, W., Z. Zuoguang, L. Yubin, L. Min, and S. Zhijie. Chemical durability and mechanical properties of alkali-proof basalt fiber and its reinforced epoxy composites. *Reinforced Plastics and Composites*, Vol. 27, No. 4, 2008, pp. 393–407.

[14] Potluri, R. Mechanical properties evaluation of T800 carbon fiber reinforced hybrid composite embedded with silicon carbide microparticles: A micromechanical approach. *Multidiscipline Modeling in Materials and Structures*, Vol. 14, No. 3, 2018, pp. 589–608.

[15] Sumida, A. and H. Mutsuyoshi. Mechanical properties of newly developed heat-resistant FRP bars. *Journal of Advanced Concrete Technology*, Vol. 6, No. 1, 2008, pp. 157–170.

[16] Wang, X., Z. Wang, Z. Wu, and F. Cheng. Shear behavior of basalt fiber reinforced polymer (FRP) and hybrid FRP rods as shear resistance members. *Construction Building Materials*, Vol. 73, 2014, pp. 781–789.

[17] Hajiloo, H., M. F. Green, and J. Gales. Mechanical properties of GFRP reinforcing bars at high temperatures. *Construction and Building Materials*, Vol. 162, 2018, pp. 142–154.

[18] Wang, Y. C., P. M. H. Wong, and V. Kodur. An experimental study of the mechanical properties of fibre reinforced polymer (FRP) and steel reinforcing bars at elevated temperatures. *Composite Structures*, Vol. 80, No. 1, 2007, pp. 131–140.

[19] Kim, H. Y., Y. H. Park, Y. J. You, and C. K. Moon. Short-term durability test for GFRP rods under various environmental conditions. *Composite Structures*, Vol. 83, No. 1, 2008, pp. 37–47.

[20] Robert, M. and B. Benmokrane. Behavior of GFRP reinforcing bars subjected to extreme temperatures. *Journal of Composites for Construction*, Vol. 14, No. 4, 2010, pp. 353–360.

[21] Sim, J. and C. Park. Characteristics of basalt fiber as a strengthening material for concrete structures. *Composites Part B: Engineering*, Vol. 36, No. 6–7, 2005, pp. 504–512.

[22] Hamad, R. J., M. M. Johari, and R. H. Haddad. Mechanical properties and bond characteristics of different fiber reinforced polymer rebars at elevated temperatures. *Construction and Building Materials*, Vol. 142, Jul 1, 2017, pp. 521–535.

[23] Militký, J. and D. Křemenáková. Compressive creep of kevlarepoxy resin linear composite. *Journal of Composites for Construction*, 1998, id. 553.

[24] Wang, X. L. and X. X. Zha. Experimental research on mechanical behavior of GFRP bars under high temperature. *Applied Mechanics Materials*, Vol. 71–78, 2011, pp. 3591–3594.

[25] Feng, P., P. Zhang, X. Meng, and L. Ye. Mechanical analysis of stress distribution in a carbon fiber-reinforced polymer rod bonding anchor. *Polymers & Polymer Composites*, Vol. 6, No. 4, 2014, pp. 1129–1143.

[26] Karvanis, K., S. Rusnáková, O. Krejčí, and M. Žaludek. Preparation, thermal analysis, and mechanical properties of basalt fiber/epoxy composites. *Polymers & Polymer Composites*, Vol. 12, No. 8, 2020, id. 1785.

[27] Li, Y., S. Yin, Y. Lu, and C. Hu. Experimental research on the mechanical properties of BFRP under high temperature. *Construction and Building Materials*, Vol. 259, 2020, id. 120591.

[28] Wang, W. and W. Xue. Accelerated aging tests for evaluations of tensile properties of GFRP rebars exposed to alkaline solution. *Building Material*, Vol. 15, No. 6, 2012, pp. 1–7.

[29] Dutta, P. K. and D. Hui. Creep rupture of a GFRP composite at elevated temperatures. *Computers and Structures*, Vol. 76, No. 1, 2000, pp. 153–161.

[30] Gu, X., X. Shen, and J. Lu. Expermental investigation on tensile mechanical properties of BFRP bars. *Journal of Southwest Jiaotong University*, Vol. 45, No. 6, 2010, pp. 1–6.
[31] Huo, B. and X. Zhang. Experimental study of mechanical properties of the BFRP bar in different diameters. *Journal of Shenyang Jianzhu University* (*Natural Science*), Vol. 27, No. 4, 2011, pp. 1–5.
[32] Myers, B., S. Beecham, and J. A. van Leeuwen. Water quality with storage in permeable pavement base course. *Proceedings of the Institution of Civil Engineers-Water Management*, Vol. 164, No. 7, 2011, pp. 361–372.
[33] Wu, G., Z. Dong, X. Wang, and Y. Zhu. Prediction of long-term performance and durability of BFRP bars under the combined effect of sustained load and corrosive solutions. *Journal of Composites for Construction*, Vol. 19, No. 3, 2015, id. 04014058.
[34] Wang, X., J. Shi, J. Liu, L. Yang, and Z. Wu. Creep behavior of basalt fiber reinforced polymer tendons for prestressing application. *Materials & Design*, Vol. 59, 2014, pp. 558–564.
[35] Li, G., J. Zhao, and Z. Wang. Fatigue behavior of glass fiber-reinforced polymer bars after elevated temperatures exposure. *Materials*, Vol. 11, No. 6, 2018, id. 16.
[36] Zhang, S., C. Wang, G. Wang, X. Wu, X. Zheng, P. He, et al. Experimental study on the shear behaviors of bolted rock joints reinforced with BFRP bars. *Chinese Journal of Rock Mechanics and Engineering*, Vol. 41, No. 4, 2022, pp. 712–724.
[37] Yuan, J., C. Ye, J. Yang, Z. Xie, J. Liu, S. Wang, et al. Experimental and numerical investigation on the deterioration mechanism for grouted rock bolts subjected to freeze–thaw cycles. *Bulletin of Engineering Geology and the Environment*, Vol. 80, No. 7, 2021, pp. 5563–5574.
[38] Mirdarsoltany, M., A. Rahai, F. Hatami, R. Homayoonmehr, and F. Abed. Investigating tensile behavior of sustainable basalt–carbon, basalt–steel, and basalt–steel-wire hybrid composite bars. *Sustainability*, Vol. 13, No. 19, 2021, id. 13.
[39] Han, Q., L. Wang, and J. Xu. Experimental research on fracture behaviors of damaged CFRP tendons: Fracture mode and failure analysis. *Construction Building Materials*, Vol. 112, 2016, pp. 1013–1024.
[40] Ghaib, M., M. Shateri, D. Thomson, and D. Svecova. Study of FRP bars under tension using acoustic emission detection technique. *Journal of Civil Structural Health Monitoring*, Vol. 8, No. 2, 2018, pp. 285–300.
[41] Gao, X., Q. Xie, W. Zhao, and Y. Hu. Experimental study on determining design parameters of non-prestressed BFRP anchor for supporting soil slope. *Journal of Highway and Transportation Research and Development*, Vol. 34, No. 7, 2017, pp. 20–28,36.
[42] Jia, X., Y. Yuan, and C. Li. Experimental study on bond behavior of new type cement grouted GFRP bolts. *Chinese Journal of Rock Mechanics and Engineering*, Vol. 10, 2006, pp. 2108–2114.
[43] Zhang, B. and B. Benmokrane. Pullout bond properties of fiber-reinforced polymer tendons to grout. *Journal of Materials in Civil Engineering*, Vol. 14, No. 5, 2002, pp. 399–408.
[44] Scott, P. and J. M. Lees. Effects of solution exposure on the combined axial-shear behaviour of unidirectional CFRP rods. *Composites Part a-Applied Science and Manufacturing*, Vol. 43, No. 9, 2012, pp. 1599–1611.
[45] Feng, J., Y. Wang, H. Wu, B. Lai, and D. Xie. Field pullout tests of basalt fiber-reinforced polymer ground anchor. *Rock and Soil Mechanics*, Vol. 40, No. 7, 2019, pp. 2563–2573.
[46] Gao, B., R. Zhang, M. He, L. Sun, C. Wang, L. Liu, et al. Effect of a multiscale reinforcement by carbon fiber surface treatment with graphene oxide/carbon nanotubes on the mechanical properties of reinforced carbon/carbon composites. *Composites Part A: Applied Science and Manufacturing*, Vol. 90, No. 11, 2016, pp. 433–440.
[47] Hung, P. Y., K. T. Lau, K. Qiao, B. Fox, and N. Hameed. Property enhancement of CFRP composites with different graphene oxide employment methods at a cryogenic temperature. *Composites Part A: Applied Science and Manufacturing*, Vol. 120, No. 5, 2019, pp. 56–63.
[48] Zhao, W., H. Wand, Y. Chen, and Y. Hu. Laboratory and field test use of BFRP anchor bolt in supporting soil slope. *Journal of Engineering Geology*, Vol. 24, No. 5, 2016, pp. 1008–1015.
[49] Wang, X., Z. Wang, Z. Wu, and F. Cheng. Shear behavior of basalt fiber reinforced polymer (FRP) and hybrid FRP rods as shear resistance members. *Construction and Building Materials*, Vol. 73, Dec 30, 2014, pp. 781–789.
[50] Herwig, A. and M. Motavalli. Load-carrying capacity of GFRP bars under combined axial force–transverse force loading. *Composites Part B Engineering*, Vol. 44, No. 1, 2013, pp. 167–171.
[51] Maranan, G., A. Manalo, B. Benmokrane, W. Karunasena, and P. Mendis. Behavior of concentrically loaded geopolymer-concrete circular columns reinforced longitudinally and transversely with GFRP bars. *Engineering Structures*, Vol. 117, 2016, pp. 422–436.
[52] Deitz, D., I. E. Harik, and H. Gesund. Physical properties of glass fiber reinforced polymer rebars in compression. *Journal of Composites for Construction*, Vol. 7, No. 4, 2003, pp. 363–366.
[53] Khan, Q. S., M. N. Sheikh, M. N. Hadi. *Tension and compression testing of fibre reinforced polymer* (*FRP*) *bars*, *Conference Proceedings of FRPRCS-12 & APFIS-2015*, Nanjing, 2015.
[54] AlAjarmeh, O., A. Manalo, B. Benmokrane, P. Vijay, W. Ferdous, and P. Mendis. Novel testing and characterization of GFRP bars in compression. *Construction Building Materials*, Vol. 225, 2019, pp. 1112–1126.
[55] Bruun, E. J. GFRP bars in structural design: Determining the compressive strength versus unbraced length interaction curve. *Journal of Student Science Technology*, Vol. 7, No. 1, 2014, pp. 16–30.
[56] Chen, J., F. He, and S. Zhang. A study of the load transfer behavior of fully grouted rock bolts with analytical modelling. *International Journal of Mining Science and Technology*, Vol. 30, No. 1, 2020, pp. 105–109.
[57] Zheng, L., L. Wang, and L. Zhu. Analytical model of shear mechanical behaviour of bolted rock joints considering influence of normal stress on bolt guide rail effect. *Journal of Central South University*, Vol. 28, No. 5, 2021, pp. 1505–1518.
[58] Won, J. P., C. G. Park, and C. I. Jang. Tensile fracture and bond properties of ductile hybrid FRP reinforcing bars. *Polymers & Polymer Composites*, Vol. 15, No. 1, 2007, pp. 9–16.

[59] Einstein, H. H. International symposium on rock bolting. *Rock Mechanics*, Vol. 12, 1984, id. 5.
[60] Spang, K. and P. Egger. Action of fully-grouted bolts in jointed rock and factors of influence. *Rock Mechanics and Rock Engineering*, Vol. 23, 1990, pp. 201–229.
[61] Dai, Y., Y. Tan, Q. Yang, Z. Wang, J. Ding, and J. Xie. Development of rapid-hardening, expansive, high-strength grouting mortar. *Journal of Civil, Architectural & Environmental Engineering*, Vol. 35, No. 4, 2013, pp. 128–132.
[62] Zhou, J., X. Wang, Z. Peng, Z. Wu, and Z. Zhu. Failure mechanism and optimization of fiber-reinforced polymer cable-anchor system based on 3D finite element model. *Engineering Structures*, Vol. 243, No. 9, 2021, id. 11.
[63] Huang, Z., G. LI, S. Wang, and W. Li. Field test on pull out behaviors of anchorage structures with glass fiber reinforced plastic rods for different surrounding rock masses. *Chinese Journal of Rock Mechanics and Engineering*, Vol. 27, No. 5, 2008, id. 11.
[64] Koller, R., S. Chang, and Y. Xi. Fiber-reinforced polymer bars under freeze-thaw cycles and different loading rates. *Journal of Composite Materials*, Vol. 41, No. 1, 2006, pp. 5–25.
[65] Dutta, P. Structural fiber composite materials for cold regions. *Journal of Cold Regions Engineering*, Vol. 2, No. 3, 1988, pp. 124–134.
[66] Saeed, Y. M., S. M. Al-Obaidi, E. G. Al-hasany, and F. N. Rad. Evaluation of a new bond-type anchorage system with expansive grout for a single FRP rod. *Construction and Building Materials*, Vol. 26111, 2020, id. 20.
[67] Verghese, K., J. Haramis, S. Patel, J. Senne, S. Case, J. Lesko. Enviro-mechanical durability of polymer composites. *Long term durability of structural materials*, *Durability 2000 Proceedings of the Durability Workshop*, Berkeley, 2001.
[68] Li, H., G. Xian, Q. Lin, and H. Zhang. Freeze–thaw resistance of unidirectional-fiber-reinforced epoxy composites. *Journal of Applied Polymer Science*, Vol. 123, No. 6, 2011, pp. 3781–3788.
[69] Wang, X., J. Lu, Z. Wang. Application of FRP screw anchor and geosynthetics in repairing of canal slope of expansive soils. *South-to-North Water Transfers and Water*, Vol. 5, 2007, pp. 127–131.
[70] Zou, W., X. Wang, and S. K. Vanapalli. Experimental evaluation of engineering properties of GFRP screw anchors for anchoring applications. *Journal of Materials in Civil Engineering*, Vol. 28, No. 7, 2016, id. 11.
[71] Wang, Y., Z. Wang, C. Shen, and Y. Wu. Research on enhancement of GFRP-anchor's torsional strength. *Science Engineering of Composite Materials*, Vol. 19, No. 4, 2012, pp. 423–429.
[72] Raja, R. S., K. Manisekar, and V. Manikandan. Study on mechanical properties of fly ash impregnated glass fiber reinforced polymer composites using mixture design analysis. *Materials & Design*, Vol. 55, 2014, pp. 499–508.
[73] Seshanandan, G., D.Ravindran, and T.Sornakumar. Mechanical properties of nano titanium oxide particles-hybrid jute-glass FRP composites. *Materials today: proceedings*, Vol. 3, No. 6, 2016, pp. 1383–1388.
[74] Han, Q., L. Wang, and J. Xu. Experimental research on mechanical properties of transverse enhanced and high-temperature-resistant CFRP tendons for prestressed structure. *Construction Building Materials*, Vol. 98, 2015, pp. 864–874.
[75] Nazir, T., A. Afzal, H. M. Siddiqi, Z. Ahmad, and M. Dumon. Thermally and mechanically superior hybrid epoxy-silica polymer films via sol-gel method. *Progress in Organic Coatings*, Vol. 69, No. 1, 2010, pp. 100–106.
[76] David, F., P. Moretti, V. Tagliaferri, and F. Trovalusci. FIMEC test to evaluate the water uptake of coated and uncoated CFRP composites. *Materials*, Vol. 13, No. 5, 2020, id. 12.
[77] Nguyen, P. N. D., M. Kubouchi, T. Sakai, S. A. Roces, F. T. Bacani, P. Yimsiri, et al. Relationship of mechanical properties and temperature of carbon fiber-reinforced plastics under microwave irradiation. *Clean Technologies and Environmental Policy*, Vol. 14, No. 5, 2012, pp. 943–951.
[78] Czigány, T. Basalt fiber reinforced hybrid polymer composites. *Materials Science Forum*, Vol. 473/474, No. 1, 2005, pp. 59–66.
[79] Protchenko, K. and E. Szmigiera. Post-fire characteristics of concrete beams reinforced with hybrid FRP bars. *Materials*, Vol. 13, No. 5, 2020, id. 1248.
[80] He, Z., M. Yu, and J. Ou. Development and experimental study of CG-FRP hybrid rebar. *Journal of Habrin Institute of Technology*, Vol. 6, 2007, pp. 845–848.
[81] Ali, N. M., X. Wang, and Z. Wu. Integrated performance of FRP tendons with fiber hybridization. *Journal of Composites for Construction*, Vol. 18, No. 3, 2013, id. 10.
[82] Colombo, C., L. Vergani, and M. Burman. Static and fatigue characterisation of new basalt fibre reinforced composites. *Composite Structures*, Vol. 94, No. 3, 2012, pp. 1165–1174.
[83] Jin, Q., P. Chen, Y. Gao, A. Du, D. Liu, and L. Sun. Tensile strength and degradation of GFRP bars under combined effects of mechanical load and alkaline solution. *Materials*, Vol. 13, No. 8, 2020, pp. 3533.3531–3533.3513.
[84] Elgabbas, F., E. A. Ahmed, and B. Benmokrane. Physical and mechanical characteristics of new basalt-FRP bars for reinforcing concrete structures. *Construction and Building Materials*, Vol. 95, No. 10, 2015, pp. 623–635.
[85] Abbasi, A. and P. Hogg. Temperature and environmental effects on glass fibre rebar: Modulus, strength and interfacial bond strength with concrete. *Composites Part B Engineering*, Vol. 36, No. 5, 2005, pp. 394–404.
[86] Ramachandran, B. E., V. Velpari, and N. Balasubramanian. Chemical durability studies on basalt fibres. *Journal of Materials Science*, Vol. 16, No. 12, 1981, pp. 3393–3397.
[87] Benmokrane, B., F. Elgabbas, E. A. Ahmed, and P. Cousin. Characterization and comparative durability study of glass/vinyl ester, basalt/vinylester, and basalt/epoxy FRP bars. *Journal of Composites for Construction*, Vol. 19, No. 6, 2015, pp. 04015008.04015001–04015008.04015012.
[88] Rybin, V. A., A.V. Utkin, and N. I. Baklanova. Alkali resistance, microstructural and mechanical performance of zirconia-coated basalt fibers. *Cement and Concrete Research*, Vol. 5311, 2013, pp. 1–8.
[89] Kim, M. T., K. Y. Rhee, B. H. Lee, and C. J. Kim. Effect of carbon nanotube addition on the wear behavior of basalt/epoxy woven composites. *Journal of Nanoscience and Nanotechnology*, Vol. 13, 2013, pp. 5631–5635.
[90] Nasir, V., H.Karimipour, F.Taheri-Behrooz, and M. M.Shokrieh. Corrosion behaviour and crack formation

mechanism of basalt fibre in sulphuric acid – ScienceDirect. *Corrosion Science*, Vol. 64, No. 11, 2012, pp. 1–7.
[91] Wei, B., H. Cao, and S. Song. Degradation of basalt fibre and glass fibre/epoxy resin composites in seawater – ScienceDirect. *Corrosion Science*, Vol. 53, No. 1, 2011, pp. 426–431.
[92] Yan, L. and N. Chouw. Effect of water, seawater and alkaline solution ageing on mechanical properties of flax fabric/epoxy composites used for civil engineering applications. *Construction and Building Materials*, Vol. 9911, 2015, pp. 118–127.
[93] Tual, N., N. Carrere, P. Davies, T. Bonnemains, and E. Lolive. Characterization of sea water ageing effects on mechanical properties of carbon/epoxy composites for tidal turbine blades. *Composites Part A: Applied Science and Manufacturing*, Vol. 78, No. 11, 2015, pp. 380–389.
[94] Abdel-Magid, B., S. Ziaee, K. Gass, and M. Schneider. The combined effects of load, moisture and temperature on the properties of E-glass/epoxy composites. *Composite Structures*, Vol. 71, No. 3/4, 2005, pp. 320–326.
[95] Tannous, F. E. and H. Saadatmanesh. Durability of AR glass fiber reinforced plastic bars. *Journal of Composites for Construction*, Vol. 3, No. 1, 1999, pp. 12–19.
[96] Wang, H., C. K. Li, and F. Guo. Experimental study on the durability of BFRP bars under the acidic solution, the cycle of freezing and thawing and the coupled actions. *Journal of Disaster Prevention and Mitigation Engineering*, Vol. 38, No. 1, 2018, pp. 39–46.
[97] Brunbauer, J. and G. Pinter. Effects of mean stress and fibre volume content on the fatigue-induced damage mechanisms in CFRP. *International Journal of Fatigue*, Vol. 75, 2015, pp. 28–38.
[98] Talreja, R. Fatigue of composite materials. In *Modern trends in composite laminates mechanics*, Springer, Berlin, 2003, 281–294.
[99] Nanni, A. Fiber-reinforced-plastic (FRP) reinforcement for concrete structures: Properties and applications. *Developments in Civil Engineering*, Vol. 16, No. 1, 1993, pp. 65–66.
[100] Demers, C. E. Fatigue strength degradation of E-glass FRP composites and carbon FRP composites. *Construction and Building Materials*, Vol. 12, No. 5, 1998, pp. 311–318.
[101] Debaiky, A. S., G. Nkurunziza, B. Benmokrane, and P. Cousin. Residual tensile properties of GFRP reinforcing bars after loading in severe environments. *Journal of Composites for Construction*, Vol. 10, No. 5, 2006, pp. 370–380.
[102] Saini, A., R. Chhibber, and A. Chattopadhyay. Effect of combined fatigue and hygrothermal loading on structural properties of E-glass/polymers. *Proceedings of the Institution of Mechanical Engineers Part C-Journal of Mechanical Engineering Science*, Vol. 231, No. 18, 2017, pp. 3382–3392.
[103] Shi, J., X. Wang, Z. Wu, and Z. Zhu. Fatigue behavior of basalt fiber-reinforced polymer tendons under a marine environment. *Construction and Building Materials*, Vol. 137, 2017, pp. 46–54.
[104] Bank, L. C., T. R. Gentry, and B. P. Thompson. A model specification for FRP composites for civil engineering structures. *SAGE*, Vol. 17, No. 6/7, 2003, pp. 405–437.
[105] Wang, X., P. Xu, Z. Wu, and J. Shi. A novel anchor method for multitendon FRP cable: Manufacturing and experimental study. *Journal of Composites for Construction*, Vol. 19, No. 6, 2015, id. 11.
[106] Xu, B. and H. Y. Li. Comparative study on expansive soil steep slope FRP materials bolt support. *Applied Mechanics and Materials*, Vol. 454, No. 10, 2013, pp. 250–254.
[107] Liu, Y. and Y. Yuan. Experimental research on anchorage performance of full-thread GFRP bonding anchor bolts. *Chinese Journal of Rock Mechanics and Engineering*, Vol. 29, No. 2, 2010, pp. 394–400.
[108] Bai, X., X. Liu, M. Zhang, D. Jing, and C. Zheng. Field tests and load-displacement models of GFRP bars and steel bars for anti-floating anchors. *Acta materiae Compositae Sinica*, Vol. 38, No. 12, 2021, id. 12.
[109] Puigvert, F., L. Gil, C. Escrig, and E. Bernat. Stress relaxation analysis of adhesively bonded anchorages for CFRP tendons. *Construction and Building Materials*, Vol. 66, No. 9, 2014, pp. 313–322.
[110] Yan, K., J. Yang, Y. Zhang, J. H. Doh, and X. Zhang. Safety performance monitoring of smart FBG-based FRP anchors. *Safety Science*, Vol. 128, No. 8, 2020, id. 10.
[111] Benmokrane, B., B. Zhang, and A. Chennouf. Tensile properties and pullout behaviour of AFRP and CFRP rods for grouted anchor applications. *Construction and Building Materials*, Vol. 14, No. 3, 2000, pp. 157–170.
[112] Feng, J., Y. Wang, Y. Zhang, L. Huang, C. He, and H. Wu. Experimental comparison of anchorage performance between basalt fiber and steel bars. *Rock and Soil Mechanics*, Vol. 40, No. 11, 2019, id. 9.
[113] Chen, C., G. Zhang, J. G. Zornberg, A. M. Morsy, and J. Huang. Interface bond behavior of tensioned glass fiber-reinforced polymer (GFRP) tendons embedded in cemented soils. *Construction and Building Materials*, Vol. 263, No. 12, 2020, id. 22.
[114] Grasselli, G. 3D behaviour of bolted rock joints: Experimental and numerical study. *International Journal of Rock Mechanics and Mining Sciences*, Vol. 42, No. 1, 2005, pp. 13–24.
[115] Biscaia, H. C., C. Chastre, C. Silva, and N. Franco. Mechanical response of anchored FRP bonded joints: A nonlinear analytical approach. *Mechanics of Advanced Materials and Structures*, Vol. 25, No. 5, 2018, pp. 238–252.
[116] Salcher, M. and R. Bertuzzi. Results of pull tests of rock bolts and cable bolts in sydney sandstone and shale. *Tunnelling and Underground Space Technology*, Vol. 74, No. 4, 2018, pp. 60–70.
[117] Xue, W. C., S. L. Zhang, and M. R. Kang. Bond strength of glass fibre-reinforced polymer ground anchors with helically wound ribs in different bonding agents. *Materials Research Innovations*, Vol. 19, No. 1, 2015, pp. 449–453.
[118] Wu, H., Z. Wu, H. Lei, and T. Lai. Application of BRFP new-type anchor cable material in high slopes against earthquakes. *Advances in Civil Engineering*, Vol. 2021, No. 4, 2021, pp. 1–19.
[119] Wu, Z., H. Wu, X. Xie, and F. Wang. Shaking table test of traditional anchorage and BFRP anchorage in high slope protection. *The Chinese Journal of Geological Hazard and Control*, Vol. 30, No. 6, 2019, pp. 94–104.

[120] Lai, T., H. Lei, Z. Wu, and H. Wu. Shaking table test study on basalt fiber reinforced plastics in high slope protection. *Rock and Soil Mechanics*, Vol. 42, No. 2, 2021, pp. 390–400.
[121] Al-Oqla, F. M. Flexural characteristics and impact rupture stress investigations of sustainable green olive leaves biocomposite materials. *Journal of Polymers and the Environment*, Vol. 29, No. 3, 2021, pp. 892–899.
[122] AL-Oqla, F. M., A. Almagableh, M. A. Omari. Design and fabrication of green biocomposites. In *Green biocomposites*, Springer, Swizerland, 2017, pp. 45–67.
[123] Al-Oqla, F., S. Sapuan, M. R. Ishak, N. A. A. Selecting natural fibers for industrial applications. *Presented at Postgraduate Symposium on Biocomposite Technology*, 2015, Vol. 2015.